Article

Current Biology

Rap1 coordinates cell-cell adhesion and cytoskeletal reorganization to drive collective cell migration *in vivo*

Highlights

- The small GTPase Rap1 directs collective cell migration for rapid wound healing
- Rap1 acts through Canoe/Afadin to reinforce tricellular adherens junctions
- Rap1 promotes Rho1/RhoA signaling to recruit myosin to the wound edge
- Adhesion and cytoskeletal remodeling generate forces to coordinate cell migration

Authors

Katheryn E. Rothenberg, Yujun Chen, Jocelyn A. McDonald, Rodrigo Fernandez-Gonzalez

Correspondence

rodrigo.fernandez.gonzalez@utoronto.ca

In brief

Rothenberg et al. demonstrate the role of the Rap1 GTPase in embryonic wound healing. Rap1 signals through Canoe/Afadin to reinforce adherens junctions around the wound and through the RhoGEF Ephexin to activate Rho1/RhoA and polarize myosin at the wound edge. Cell adhesion and cytoskeletal remodeling coordinate cell movements for rapid wound repair.

Rothenberg et al., 2023, Current Biology *33*, 2587–2601
July 10, 2023
https://doi.org/10.1016/j.cub.2023.05.009

CellPress

Current Biology

CellPress

Article

Rap1 coordinates cell-cell adhesion and cytoskeletal reorganization to drive collective cell migration *in vivo*

Katheryn E. Rothenberg,[1,2] Yujun Chen,[3] Jocelyn A. McDonald,[3] and Rodrigo Fernandez-Gonzalez[1,2,4,5,6,7,*]
[1]Institute of Biomedical Engineering, University of Toronto, Toronto, ON M5S 3G9, Canada
[2]Translational Biology and Engineering Program, Ted Rogers Centre for Heart Research, University of Toronto, Toronto, ON M5G 1M1, Canada
[3]Division of Biology, Kansas State University, Manhattan, KS 66506, USA
[4]Department of Cell and Systems Biology, University of Toronto, Toronto, ON M5S 3G5, Canada
[5]Developmental and Stem Cell Biology Program, The Hospital for Sick Children, Toronto, ON M5G 1X8, Canada
[6]Twitter: @rfg_lab
[7]Lead contact
*Correspondence: rodrigo.fernandez.gonzalez@utoronto.ca
https://doi.org/10.1016/j.cub.2023.05.009

SUMMARY

Collective cell movements contribute to tissue development and repair and spread metastatic disease. In epithelia, cohesive cell movements require reorganization of adherens junctions and the actomyosin cytoskeleton. However, the mechanisms that coordinate cell-cell adhesion and cytoskeletal remodeling during collective cell migration *in vivo* are unclear. We investigated the mechanisms of collective cell migration during epidermal wound healing in *Drosophila* embryos. Upon wounding, the cells adjacent to the wound internalize cell-cell adhesion molecules and polarize actin and the motor protein non-muscle myosin II to form a supracellular cable around the wound that coordinates cell movements. The cable anchors at former tricellular junctions (TCJs) along the wound edge, and TCJs are reinforced during wound closure. We found that the small GTPase Rap1 was necessary and sufficient for rapid wound repair. Rap1 promoted myosin polarization to the wound edge and E-cadherin accumulation at TCJs. Using embryos expressing a mutant form of the Rap1 effector Canoe/Afadin that cannot bind Rap1, we found that Rap1 signals through Canoe for adherens junction remodeling, but not for actomyosin cable assembly. Instead, Rap1 was necessary and sufficient for RhoA/Rho1 activation at the wound edge. The RhoGEF Ephexin localized to the wound edge in a Rap1-dependent manner, and Ephexin was necessary for myosin polarization and rapid wound repair, but not for E-cadherin redistribution. Together, our data show that Rap1 coordinates the molecular rearrangements that drive embryonic wound healing, promoting actomyosin cable assembly through Ephexin-Rho1, and E-cadherin redistribution through Canoe, thus enabling rapid collective cell migration *in vivo*.

INTRODUCTION

Collective cell migration is a fundamental cell behavior in development and disease.[1,2] Sculpting of tissues during embryonic development relies on the ability of cells to move cohesively in a directed manner, such as during dorsal closure in *Drosophila*[3–5] and gastrulation and neurulation in vertebrates.[6–8] Coordinated cell movements also contribute to cancer metastasis.[1,9,10] Despite their importance, major gaps remain in our understanding of the molecular mechanisms that initiate and drive collective cell migration, thus precluding the identification of therapeutic targets that could be used to prevent or treat congenital disorders and cancer metastasis.

Embryos of many species have a remarkable ability to heal wounds rapidly and without scarring in a process driven by collective cell movements.[4,5,11–14] Reorganization of cell-cell adhesions and the cytoskeleton facilitates the coordinated movement of cells to repair embryonic tissues.[15] Shortly after wounding, adherens junction components including E-cadherin, α-catenin, and β-catenin are endocytosed from the wound edge and accumulate at former tricellular junctions (TCJs) along the wound perimeter.[5,16–20] Simultaneously, actin and the motor protein non-muscle myosin II are polarized to the wound edge and form a contractile supracellular cable.[4,5,11,13,16,17] Actin and myosin are initially heterogeneously distributed around the wound, allowing for segments of the wound edge with high actomyosin accumulation to contract and generate mechanical strain on neighboring segments, which drives additional cytoskeletal recruitment.[14,18] Over time, cable heterogeneity decreases as all cell junctions at the wound edge accumulate actin and myosin. Calcium release upon wounding and the subsequent production of reactive oxygen species (ROS) initiate junctional and cytoskeletal remodeling at the leading edge.[19,21–23] However, we still do not understand how

mechanical and chemical signals are sensed, integrated, or translated into the molecular rearrangements that drive wound healing.

The small GTPase Rap1 could integrate mechanical and chemical signals during embryonic wound repair. Rap1 is sensitive to ROS via its activator, the guanine nucleotide exchange factor (GEF) Epac,[24] and to mechanical signals via its GEF C3G,[25] suggesting that Rap1 could be activated by signals associated with tissue damage. Rap1 also plays a role in adherens junction formation and maintenance,[26–31] tissue integrity preservation,[32] and cytoskeletal reorganization.[28,30,33] The adherens junction protein Canoe/Afadin is a known effector of the small GTPase Rap1 that interacts with adherens junctions under tension.[31,34,35] Additionally, Rap1 is a marker of highly metastatic cancers.[36–38] Therefore, Rap1 is a strong candidate for acting as a signaling nexus during collective cell migration. Here, we investigate the role of Rap1 in *Drosophila* embryonic wound healing and how Rap1 coordinates cell adhesion and cytoskeletal rearrangements to drive collective cell movement.

RESULTS

Adherens junctions and Rap1 localize simultaneously to TCJs around wounds

Rap1 drives adherens junction formation and remodeling during *Drosophila* embryonic development. To investigate if Rap1 is involved in junctional redistribution during *Drosophila* embryonic wound healing, we quantified the dynamics of adherens junction proteins and Rap1 dynamics during wound repair. Consistent with previous reports,[5,17–20] we found that junctional proteins were depleted from bicellular junctions (BCJs) at the wound edge, between a wounded cell and a cell adjacent to the wound, and accumulated at TCJs around the wound. During the first 15 min of wound closure, DE-cadherin:tdTomato[39] fluorescence at BCJs decreased by 16% ± 7% (mean ± SEM) with respect to pre-wound levels ($p = 0.010$) and increased by 17% ± 5% at TCJs ($p = 0.005$; Figures 1A–1A″). α-catenin:GFP[40] levels decreased by 8% ± 7% at BCJs and accumulated by 33% ± 8% at TCJs ($p = 7.2 \times 10^{-5}$; Figures 1B–1B″). Finally, Canoe:YFP[41,42] decreased by 30% ± 10% at BCJs ($p = 0.011$) and increased by 30% ± 9% at TCJs ($p = 0.002$; Figures 1C–1C″). Notably, Rap1:GFP[26] accumulated at the edge of wounds and particularly at TCJs, where Rap1:GFP fluorescence increased by 60% ± 12% ($p = 6.6 \times 10^{-6}$; Figures 1D–1D″). Our results indicate that Rap1 is polarized to the wound edge, where Rap1 displays a strong localization to TCJs.

To measure whether Rap1 is active at the wound edge, we developed a biosensor for Rap1 activity composed of the two Rap1-binding domains of Canoe, RA1 and RA2[34] (Figures S1A–S1C). The linker region between RA1 and RA2 contains a predicted NLS site, which retained the RA1 and RA2 domains in the nucleus (Figures S1A–S1C). Thus, our design for the biosensor involved excision of the predicted NLS site, tagging at the N terminus with eGFP, and placing the sensor under the control of a UAS promoter (Figure S1B). The sensor was tested in *Drosophila* S2R+ cells in culture,[43] in which the sensor localized in the cytosol (Figure S1C). In contrast, in cells expressing a constitutively active Rap1 construct (Rap1CA), the sensor co-localized with Rap1CA at discrete membrane structures (Figure S1C′). In wounded embryos, the biosensor displayed a 2.3- ± 0.2-fold increase in fluorescence at the wound edge 15 min after wounding (Figures S1D–S1F), an increase that was abolished when we disrupted Rap1 activity using a Rap1 dominant-negative construct (Rap1DN)[44] using the UAS-Gal4 system[45] and *tubulin-Gal4* to drive Rap1DN expression throughout the embryo ($p = 0.027$; Figures S1E and S1F). Together, our results indicate that Rap1 is active at the wound edge and colocalizes with its effector Canoe at TCJs, suggesting that Rap1 may promote TCJ formation during embryonic wound closure.

Rap1 is required for the molecular rearrangements that drive rapid wound healing

To determine if Rap1 is necessary for rapid wound closure, we disrupted Rap1 activity in the epidermis of *Drosophila* embryos by overexpressing Rap1DN using the UAS-Gal4 system and *daughterless-Gal4* as the driver to bypass early development. Embryos also expressed DE-cadherin:tdTomato and the myosin regulatory light chain (a subunit of the myosin II motor; encoded for by the *sqh* gene in *Drosophila*) tagged with GFP.[46] Rap1DN slowed the rate of wound closure by 49% with respect to controls ($p = 0.033$; Figures 2A–2D; Video S1). We quantified a similar 47% reduction in the wound closure rate when we knocked down Rap1 using the UAS-Gal4 system to express RNAi against *rap1* ($p = 0.038$; Figures S2A–S2D), as well as a 64% reduction in the closure rate when we measured the effects of overexpressing Rap1DN using an alternative myosin marker, the myosin heavy chain (Zipper) tagged with GFP[47] ($p = 0.02$; Figures S3A–S3D). Together, our results indicate that Rap1 is necessary for rapid embryonic wound repair.

To investigate the mechanisms by which Rap1 controls wound closure, we measured the dynamics of junctional and cytoskeletal proteins around the wound when Rap1 signaling was disrupted. DE-cadherin intensity at cell-cell interfaces in pre-wounded cells was not affected by Rap1DN (Figures 2A, 2B, 2E, S1D, and S1E) or by *rap1* RNAi (Figures S2A, S2B, and S2E). DE-cadherin was still removed from BCJs at the wound edge in Rap1DN embryos (37% ± 7% decrease in controls versus 38% ± 6% in Rap1DN embryos; Figures 2A′, 2B′, and 2F). However, the accumulation of DE-cadherin at TCJs was disrupted in Rap1DN embryos: in controls DE-cadherin fluorescence at TCJs increased (20% ± 7% 15 min after wounding), while in Rap1DN embryos DE-cadherin fluorescence at TCJs decreased (−22% ± 4%, $p = 4 \times 10^{-6}$ relative to controls; Figures 2A′, 2B′, and 2G). We found similar defects in DE-cadherin redistribution in *rap1* RNAi embryos, in which E-cadherin was normally removed from BCJs but did not accumulate at TCJs (16% ± 6% increase in *mcherry* RNAi versus 11% ± 4% decrease in *rap1* RNAi, $p = 0.006$; Figures S2A′, S2B′, S2F, and S2G). Consistent with our results with E-cadherin, when we measured Canoe localization in Rap1DN embryos we found that Rap1 disruption did not significantly affect Canoe intensity changes at BCJs (15% ± 9% decrease in controls versus 6% ± 13% decrease in Rap1DN embryos; Figures S4A–S4C) but caused a defect in Canoe accumulation to TCJs (27% ± 7% increase in controls versus 10% ± 7% decrease in Rap1DN embryos, $p = 4 \times 10^{-6}$; Figures S4A, S4B, and S4D). Our results suggest that Rap1 is necessary for TCJ assembly during embryonic wound closure.

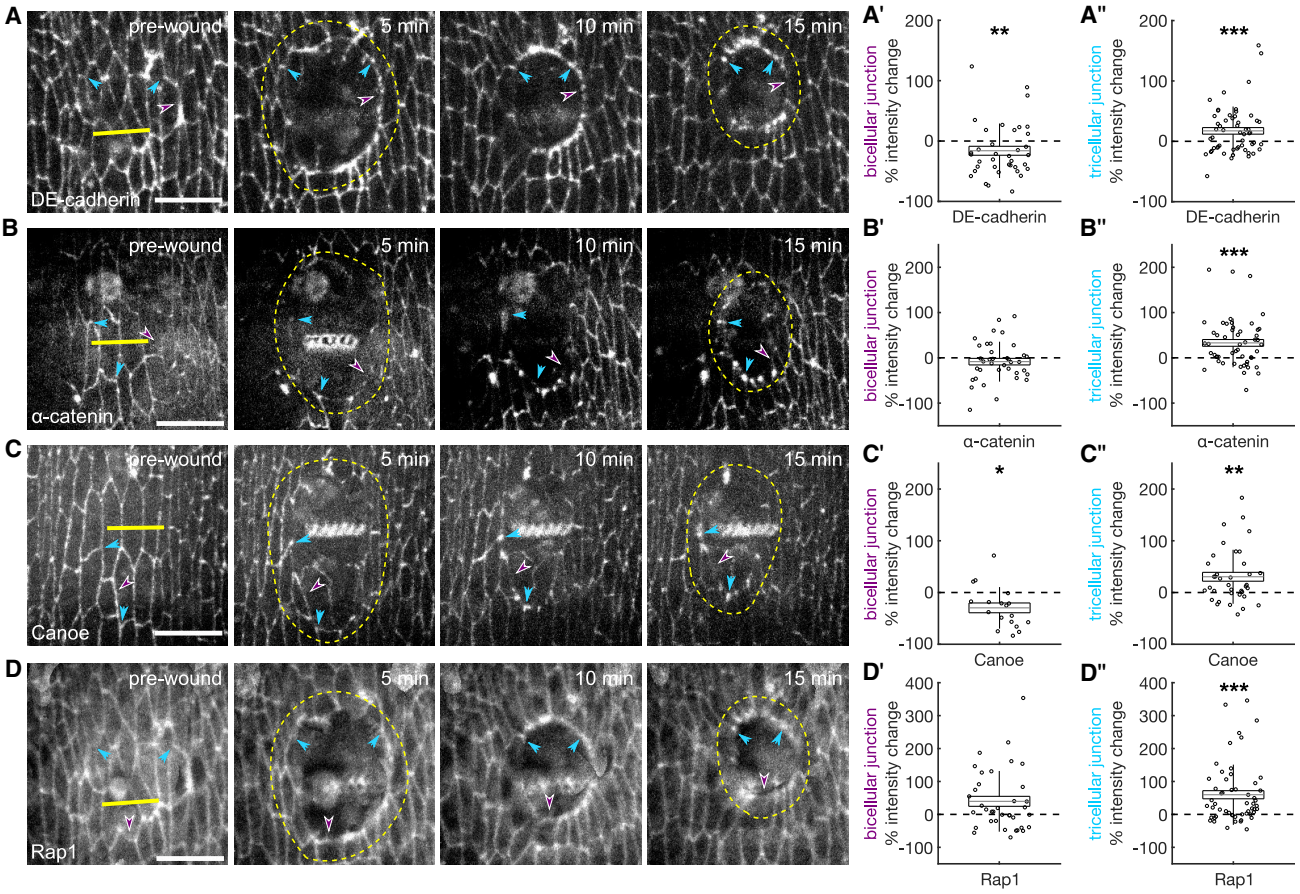

Figure 1. Rap1 localizes at the wound edge and colocalizes with adherens junctions at TCJs

(A–D) Epidermal cells in wounded embryos expressing DE-cadherin:tdTomato (A), α-catenin:GFP (B), Canoe:YFP (C), or Rap1:GFP (D). Yellow lines denote wound sites, yellow dashed lines indicate the wound edge, purple arrowheads indicate BCJs, and cyan arrowheads indicate TCJs. Time after wounding is shown. Anterior left, dorsal up. Scale bars, 15 μm.

(A′–D″) Percent fluorescence change relative to pre-wound levels at BCJs (A′–D′) and TCJs (A″–D″) 15 min post-wounding for DE-cadherin:tdTomato (A′ and A″, n = 44 BCJs and n = 65 TCJs from 6 embryos), α-catenin:GFP (B′ and B″, n = 37 BCJs and n = 52 TCJs from 5 embryos), Canoe:YFP (C′ and C″, n = 18 BCJs, and n = 37 TCJs from 5 embryos), or GFP:Rap1 (D′ and D″, n = 37 BCJs and n = 65 TCJs from 6 embryos).

Error bars, SD; boxes, SEM; gray lines, mean. *p < 0.05, **p < 0.01, ***p < 0.001, Wilcoxon signed-rank test.

See also Figure S1.

Delays in wound healing are often associated with defects in cytoskeletal dynamics around the wound. When we quantified myosin dynamics, we found that the maximum myosin accumulation at the wound edge was 46% lower in Rap1DN embryos with respect to controls when imaging Sqh (p = 0.012; Figures 2A, 2B, 2H, and 2I) and 33% lower when imaging Zipper (p = 0.045; Figures S3A, S3B, S3E, and S3F). We obtained similar results in *rap1* RNAi embryos, in which maximum myosin levels at the wound edge were 40% lower than in controls (p = 0.038; Figures S2A, S2B, S2H, and S2I). Additionally, the distribution of myosin at the wound edge was affected in Rap1DN embryos. In controls, myosin heterogeneity peaked around 5 min post-wounding and then decreased significantly by 20 min post-wounding, when myosin had been recruited to the entire wound edge (p = 0.031; Figure S5A). In Rap1DN embryos myosin heterogeneity did not significantly decrease by 20 min post-wounding (Figure S5A). Together, these results indicate that Rap1 is necessary for myosin polarization and dynamics throughout the wound healing response.

Rap1 activation accelerates wound repair and enhances myosin polarization

To investigate if Rap1 activity is sufficient to accelerate wound closure, we used the UAS-Gal4 system to overexpress constitutively active Rap1 (Rap1CA).[44] Strikingly, Rap1CA accelerated wound closure by 77% with respect to controls in embryos expressing DE-cadherin:tdTomato and Sqh:GFP (p = 0.03; Figures 3A–3D; Video S2), and by 71% in embryos expressing Zipper:GFP (p = 0.02; Figures S3G–S3J). To determine if the acceleration in wound closure in Rap1CA embryos was associated with changes in the molecular rearrangements that drive wound healing, we measured the intensity of DE-cadherin at BCJs and TCJs at the wound edge. We found no significant difference with respect to controls in DE-cadherin levels before wounding (Figures 3A, 3B, and 3E) or at either

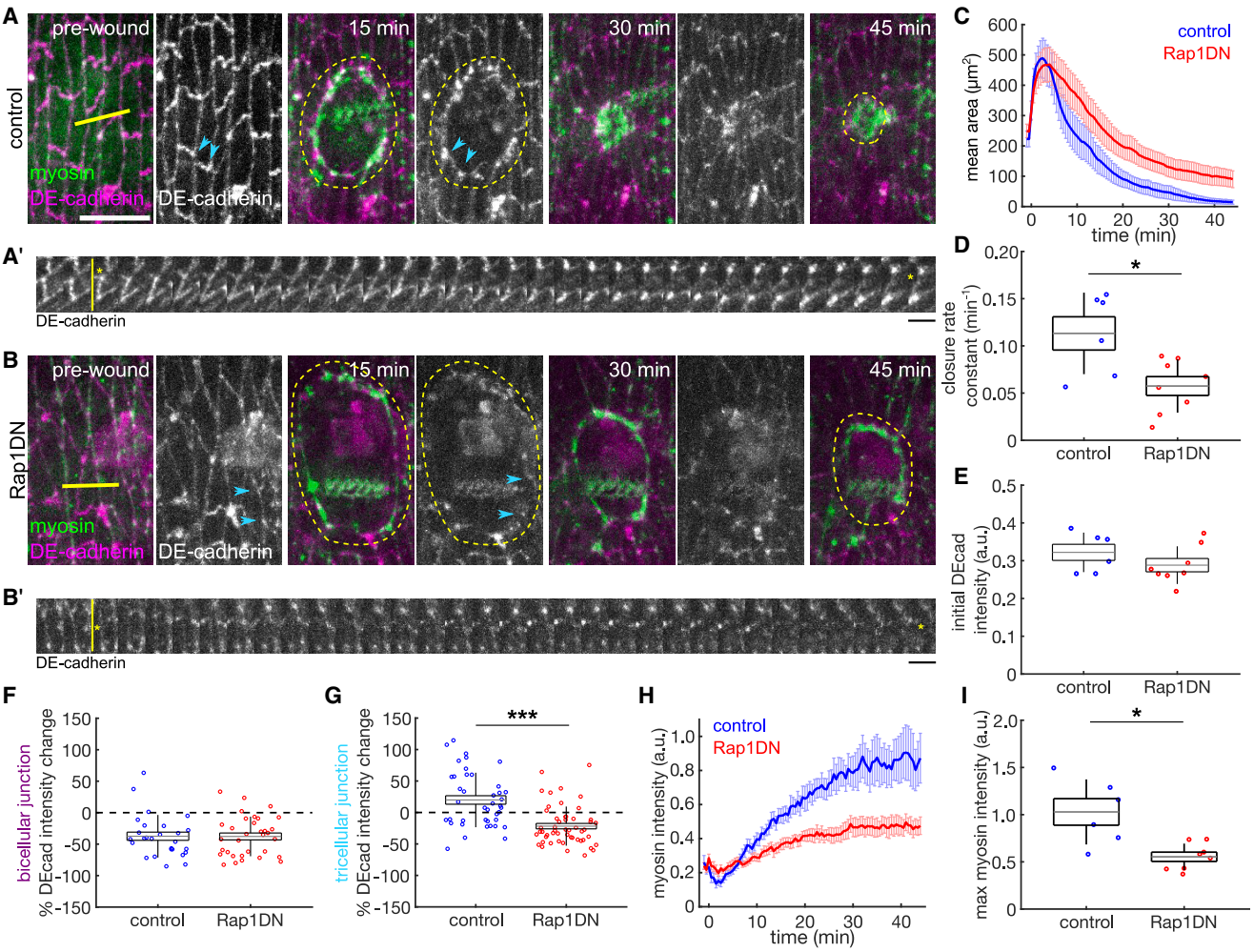

Figure 2. Rap1 is required for rapid wound closure and remodeling of cell-cell adhesions and the cytoskeleton

(A and B) Epidermal cells in wounded control (*daGal4* × *yw*, A) and Rap1DN (*daGal4* × *UAS-Rap1DN*, B) embryos expressing DE-cadherin:tdTomato (magenta and grayscale) and Sqh:GFP (green). Yellow lines denote wound sites and yellow dashed lines indicate the wound edge. Cyan arrowheads indicate TCJs flanking the BCJs shown in (A′) and (B′). Anterior left, dorsal up. Scale bar, 15 μm.

(A′ and B′) Kymographs of a TCJ pair and connecting BCJ from control (A′) and Rap1DN (B′) embryos. Yellow lines denote time of wounding and yellow asterisks show location of the wound relative to the cell junction. Scale bars, 30 s.

(C–E) Wound area over time (C), wound closure rate constant (D), and DE-cadherin intensity at cell boundaries prior to wounding (E) in control (n = 6, blue) and Rap1DN (n = 8, red) embryos.

(F and G) Percent DE-cadherin intensity change 15 min post-wounding at BCJs at the wound edge (F) or at TCJs (G), in controls (n = 27 BCJs and 41 TCJs in 6 embryos) and in Rap1DN (n = 33 BCJs and 52 TCJs in 8 embryos).

(H and I) Myosin fluorescence at the wound edge (H), and maximum myosin accumulation at the wound edge (I) in control (n = 6, blue) and Rap1DN (n = 8, red) embryos.

(C and H) Error bars, SEM.

(D–G and I) Error bars, SD; boxes, SEM; gray lines, mean. *p < 0.05, ***p < 0.001, Mann-Whitney U test.

See also Figures S2–S5 and Video S1.

BCJs or TCJs during the first 15 min following wounding (Figures 3A′, 3B′, 3F, and 3G). In contrast, myosin polarization to the wound edge was significantly impacted, with 54% greater maximum myosin accumulation after wounding in Rap1CA embryos as compared with controls (p = 0.023; Figures 3H and 3I). The dynamics of myosin remodeling were also accelerated in Rap1CA embryos: 20 min post-wounding, Rap1CA wounds displayed 30% lower Sqh:GFP heterogeneity than controls (p = 0.027; Figure S5B), suggesting faster accumulation of myosin to the wound edge, which was also evident using Zipper:GFP (Figures S3K and S3L). Together, these data show that Rap1 is sufficient for the polarization of myosin to the wound margin, contributing to rapid wound repair. The lack of effect of Rap1CA on DE-cadherin redistribution suggests that either DE-cadherin localization to TCJs is maximal in controls or that Rap1 regulates cell adhesions and the actomyosin cytoskeleton through different mechanisms.

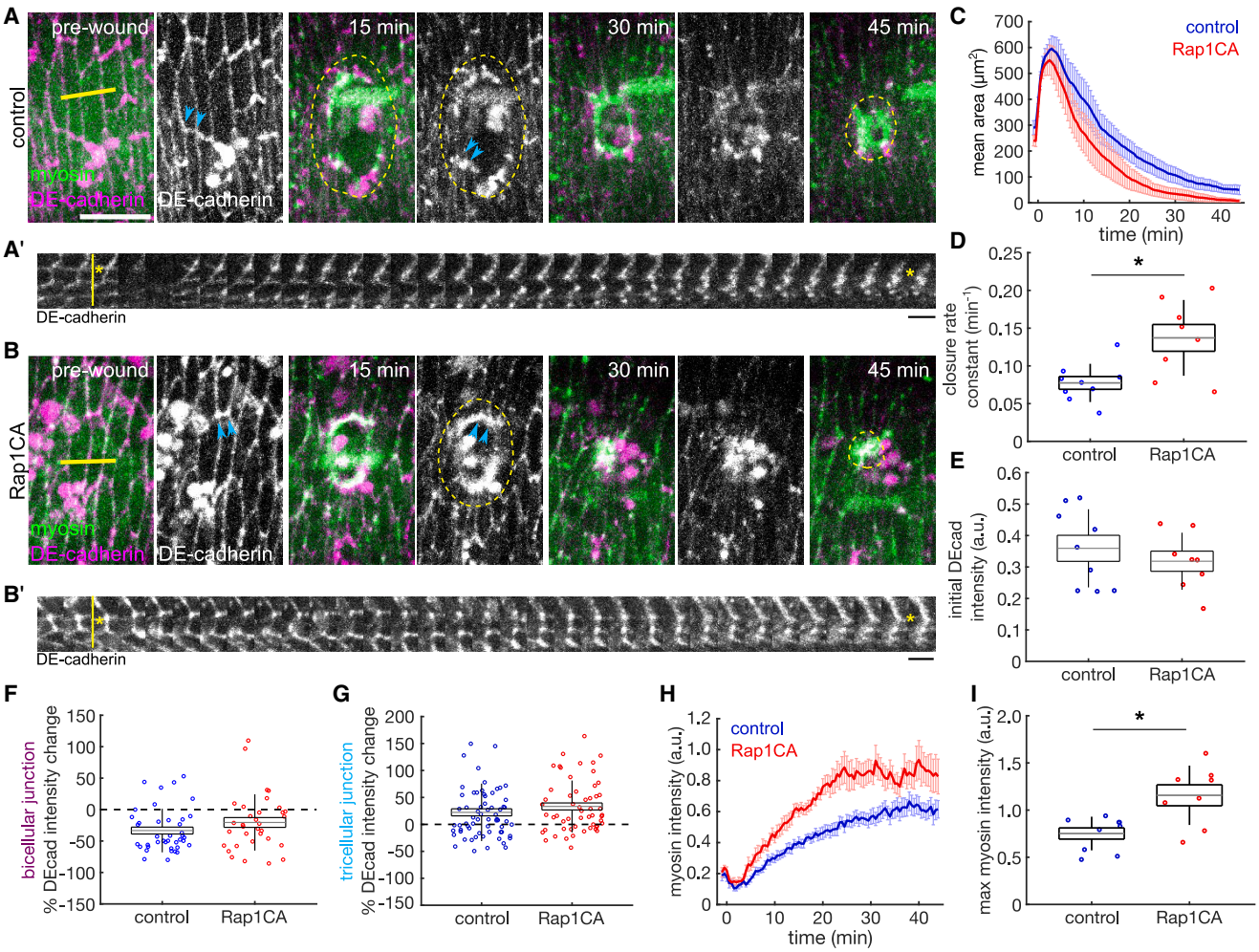

Figure 3. Increased Rap1 activity accelerates myosin polarization to the wound edge and tissue repair

(A and B) Epidermal cells in wounded control (*daGal4* × *yw*, A) and Rap1CA (*daGal4* × *UAS-Rap1CA*, B) embryos expressing DE-cadherin:tdTomato (magenta and grayscale) and Sqh:GFP (green). Yellow lines denote wound sites and yellow dashed lines indicate the wound edge. Cyan arrowheads indicate TCJs flanking the BCJs shown in (A′) and (B′). Anterior left, dorsal up. Scale bar, 15 μm.

(A′ and B′) Kymographs of a TCJ pair and connecting BCJ from control (A′) and Rap1CA (B′) embryos. Yellow lines denote time of wounding and yellow asterisks show location of the wound relative to the cell junction. Scale bars, 30 s.

(C–E) Wound area over time (C), wound closure rate constant (D), and DE-cadherin intensity at cell boundaries prior to wounding (E) in control (n = 9, blue) and Rap1CA (n = 8, red) embryos.

(F and G) Percent DE-cadherin intensity change 15 min post-wounding at BCJs at the wound edge (F) or at TCJs (G) in controls (n = 40 BCJs and 66 TCJs in 9 embryos) and in Rap1CA (n = 33 BCJs and 54 TCJs in 8 embryos).

(H and I) Myosin fluorescence at the wound edge (H), and maximum myosin accumulation at the wound edge (I) in control (n = 9, blue) and Rap1CA (n = 8, red) embryos.

(C and H) Error bars, SEM.

(D–G and I) Error bars, SD; boxes, SEM; gray lines, mean. *p < 0.05, Mann-Whitney U test.

See also Figures S3–S5 and Video S2.

Canoe is required for the junctional and cytoskeletal rearrangements that drive rapid wound closure

To further investigate how Rap1 controls junctional and cytoskeletal rearrangements during wound healing, we used the UAS-Gal4 system to express RNAi against the Rap1 effector *canoe*[29,48] in embryos expressing DE-cadherin:tdTomato and myosin:GFP. Controls expressed RNAi against *mcherry*. Using *daughterless-Gal4*, we measured a 47% reduction in Canoe at cell boundaries in embryos expressing *canoe* RNAi ($p = 1 \times 10^{-4}$; Figures S4E and S4G). Canoe knockdown slowed down wound closure by 40% (p = 0.028; Figures 4A–4D). Disruption of Canoe significantly reduced DE-cadherin localization to cell boundaries in unwounded embryos (p = 0.010; Figures 4A, 4B, and 4E) and had a striking effect on DE-cadherin dynamics at both BCJs and TCJs around the wound. In Canoe knockdowns, DE-cadherin at BCJs decreased significantly more than in controls (19% ± 7% reduction 15 min after wounding in controls versus 49% ± 4% in *canoe* RNAi embryos, p = 0.001;

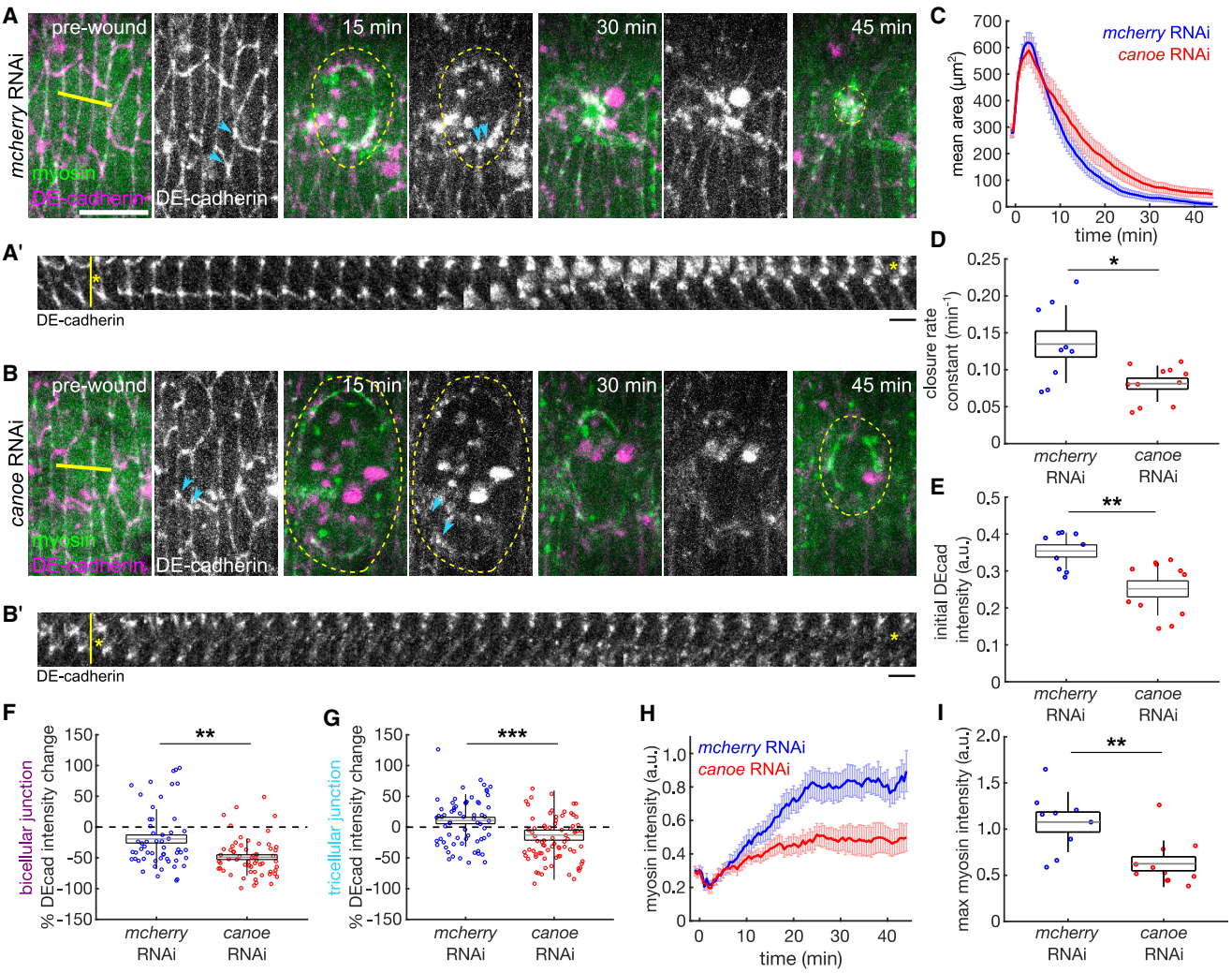

Figure 4. Canoe is required for the junctional and cytoskeletal rearrangements that drive rapid wound closure

(A and B) Epidermal cells in wounded control (*daGal4* × *UAS-mcherryRNAi*, A) and *canoe* RNAi (*daGal4* × *UAS-canoeRNAi*, B) embryos expressing DE-cadherin:tdTomato (magenta and grayscale) and Sqh:GFP (green). Yellow lines denote wound sites and yellow dashed lines indicate the wound edge. Cyan arrowheads indicate TCJs flanking the BCJs shown in (A′) and (B′). Anterior left, dorsal up. Scale bar, 15 μm.

(A′ and B′) Kymographs of a TCJ pair and connecting BCJ from control (A′) and *canoe* RNAi (B′) embryos. Yellow lines denote time of wounding and yellow asterisks show location of the wound relative to the cell junction. Scale bars, 30 s.

(C–E) Wound area over time (C), wound closure rate constant (D), and DE-cadherin intensity at cell boundaries prior to wounding (E) in control (n = 9, blue) and *canoe* RNAi (n = 11, red) embryos.

(F and G) Percent DE-cadherin intensity change 15 min post-wounding at BCJs at the wound edge (F) or at TCJs (G) in controls (n = 55 BCJs and 67 TCJs in 9 embryos) and in *canoe* RNAi (n = 61 BCJs and 78 TCJs in 8 embryos).

(H and I) Myosin fluorescence at the wound edge (H), and maximum myosin accumulation at the wound edge (I) in control (n = 9, blue) and *canoe* RNAi (n = 11, red) embryos.

(C and H) Error bars, SEM.

(D–G and I) Error bars, SD; boxes, SEM; gray lines, mean. *p < 0.05, **p < 0.01, ***p < 0.001, Mann-Whitney U test.

See also Figures S4 and S5.

Figures 4A′, 4B′, and 4F). Additionally, accumulation of DE-cadherin at TCJs was abolished in *canoe* RNAi embryos (11% ± 5% increase in controls versus 13% ± 8% decrease in *canoe* RNAi, $p = 2 \times 10^{-4}$; Figures 4A′, 4B′, and 4G). E-cadherin redistribution defects were accompanied by a 42% reduction in maximum myosin recruitment to the wound edge (p = 0.005; Figures 4H and 4I) and a defect in the resolution of myosin heterogeneity as wound closure progressed (p = 0.010; Figure S5C). Together, these results demonstrate a role for Canoe in driving rapid wound closure by promoting both adherens junction stability and redistribution, as well as cytoskeletal polarization.

Rap1 acts through Canoe to build TCJs at the wound edge

Canoe has functions independent of the confirmed Rap1-binding (RA) domains.[29,31] To determine which roles of Rap1

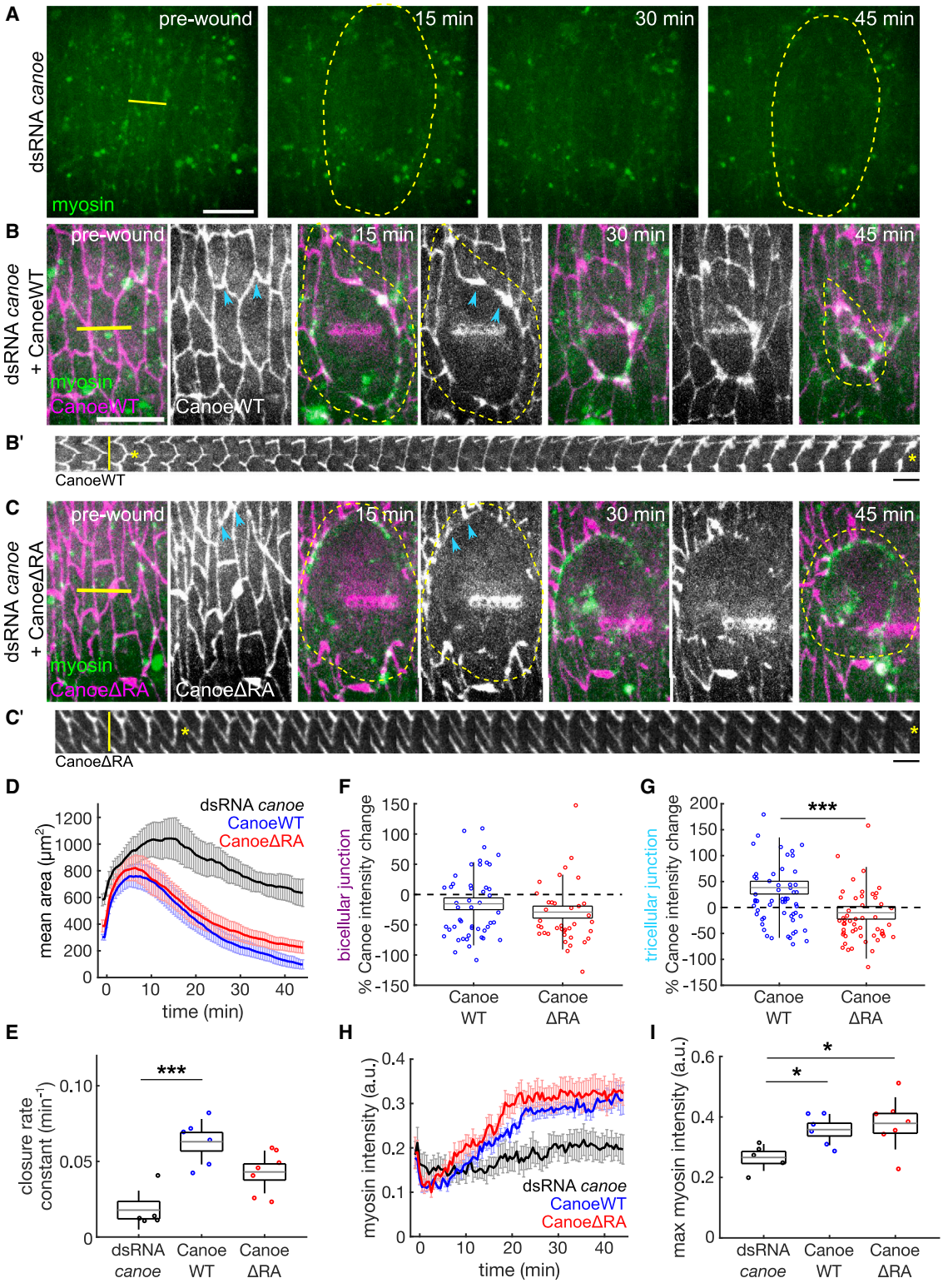

Figure 5. Rap1-Canoe interaction is necessary for TCJ formation at the wound edge and rapid wound healing

(A–C) Epidermal cells in wounded embryos expressing Sqh:mCherry (green), injected with dsRNA against *canoe* (*daGal4* × *yw*, A) and expressing CanoeWT:Venus (*daGal4* × *UAS-CanoeWT:Venus*, B) or CanoeΔRA:Venus (*daGal4* × *UAS-Canoe* Δ *RA:Venus*, C) (magenta and grayscale). Yellow lines denote wound sites and yellow dashed lines indicate the wound edge. Cyan arrowheads indicate TCJs flanking the BCJs shown in (B′) and (C′). Anterior left, dorsal up. Scale bars, 15 μm.

(legend continued on next page)

in wound closure require binding Canoe through the RA domains, we investigated the effect on wound healing of a form of Canoe that lacks the RA domains.[29] To this end, we knocked down endogenous Canoe using syncytial double-stranded RNA (dsRNA) injections (Figure 5A), and we used the UAS-Gal4 system to express wild-type Canoe (CanoeWT; Figure 5B) or a form of Canoe lacking the Rap1-binding domains (CanoeΔRA; Figure 5C).[29] The rescue constructs were dsRNA-resistant and tagged with mVenus.[35] All embryos expressed myosin:mCherry.[49] dsRNA knockdown reduced Canoe levels at cell contacts by 34% ($p = 1 \times 10^{-4}$; Figures S4F and S4H). Consistent with our results using *canoe* RNAi, *canoe* dsRNA slowed wound closure and disrupted myosin polarization to the wound edge (Figures 5A, 5D, 5E, 5H, and 5I; Video S3, left). CanoeWT accelerated the rate of closure 3.5-fold with respect to *canoe* dsRNA ($p = 9 \times 10^{-4}$; Figures 5A–5E; Video S3, center). CanoeΔRA had a milder effect and accelerated the rate of closure with respect to dsRNA embryos by 2.4-fold (p = 0.06, CanoeΔRA versus *canoe* dsRNA), a 32% smaller effect than that of CanoeWT (p = 0.1, CanoeΔRA versus CanoeWT; Figures 5A–5E; Video S3, right). These results indicate that the interaction between Rap1 and Canoe is at least in part necessary for rapid wound healing.

To determine the molecular mechanisms by which Rap1-binding affects the function of Canoe during wound healing, we quantified junctional and cytoskeletal dynamics. We used CanoeWT and CanoeΔRA fluorescence to track the redistribution of adherens junctions. CanoeΔRA depletion from BCJs at the wound edge was similar to that of CanoeWT (Figures 5B′, 5C′, and 5F), suggesting that Rap1-Canoe interaction is dispensable for junctional disassembly during wound closure. In contrast, while CanoeWT increased at TCJs at the wound edge (38% ± 12% higher 15 min after wounding, p = 0.005; Figures 5B′ and 5G), CanoeΔRA levels decreased (10% ± 12% lower, p = 0.003; Figures 5C′ and 5G), indicating that the Rap1-Canoe interaction is necessary to localize Canoe at TCJs around the wound. Strikingly, the Rap1-binding domains of Canoe were dispensable for the accumulation of myosin around the wound, as both CanoeWT and CanoeΔRA embryos displayed maximum myosin accumulations 35% and 42% greater than *canoe* dsRNA, respectively (Figures 5A–5C, 5H, and 5I); and myosin heterogeneity resolved similarly in both CanoeWT and CanoeΔRA embryos as the wound closed (Figure S5D). Overall, our results suggest that Canoe acts downstream of Rap1 to build TCJs during wound healing but not to polarize myosin to the wound edge.

Rap1 regulates Rho1 activity and force generation during embryonic wound closure

To determine how Rap1 affects myosin localization we investigated a potential interplay with the small GTPase Rho1, which is responsible for myosin polarization at the wound edge.[5,17] To test whether Rho1 activity is regulated by Rap1, we measured the dynamics during wound closure of a Rho sensor based on the GFP-tagged Rho1-binding domain of the Rho1 effector Anillin.[50] Embryos co-expressed DE-cadherin:tdTomato to track the wound margin. We found that Rho1 was activated at the wound edge in large puncta (Figure 6A). We confirmed that the AnillinRBD Rho1 sensor could detect changes in Rho1 activity using embryos expressing Rho1N19,[51] a dominant-negative form of Rho1, which led to a significant decrease in AnillinRBD levels at the wound edge (Figures S6A–S6D). We also found Rho1 puncta at the wound edge using alternative Rho1 activity sensors based on the Rho1-binding domain of the formin Diaphanous[52] or on a kinase-dead form of the kinase Rho-kinase[53] (Figures S6E and S6F).

We measured Rho1 activity in response to Rap1 manipulations. In controls, Rho1 activity at the wound edge increased by up to 3.9-fold within the first 30 min of wound closure relative to initial levels (p = 0.03; Figures 6A, 6D, and 6E; Video S4, left). In Rap1DN embryos Rho1 activity around the wound increased modestly, but significantly less than in controls (1.9-fold increase, p = 0.036 relative to controls; Figures 6B, 6D, and 6E; Video S4, center). Activation of Rap1 with Rap1CA increased Rho1 activity to an average maximum of 6.3-fold relative to initial levels (Figures 6C–6E; Video S4, right). Together, our data indicate that Rap1 controls Rho1 activity in response to wounding.

To determine if Rap1 controls force generation around the wound, we measured recoil velocity following single point laser ablation of the myosin cable at the wound edge 10 min after wounding. Rap1DN embryos displayed a 31% reduction in the recoil velocity after ablation relative to controls (p = 0.028), while Rap1CA embryos showed a 36% increase compared with controls (p = 0.038; Figures 6F–6I; Video S5). We used a Kelvin-Voigt mechanical-equivalent model to estimate the viscosity to elasticity ratio at the wound edge using the time-dependent relaxation following laser ablation,[54] and we found no significant differences between controls, Rap1DN, and Rap1CA embryos (Figure 6J), indicating that differences in recoil velocity after laser ablation can be attributed to differences in tension at the cable. Together, our results reveal that Rap1 is both necessary and sufficient for the generation of tension around embryonic wounds.

(B′ and C′) Kymographs of a TCJ pair and connecting BCJ from CanoeWT (B′) and CanoeΔRA (C′) embryos. Yellow lines denote time of wounding and yellow asterisks show location of the wound relative to the cell junction. Scale bars, 30 s.
(D and E) Wound area over time (D), and wound closure rate constant (E) in dsRNA *canoe* (n = 5, black), CanoeWT (n = 6, blue) and CanoeΔRA (n = 7, red) embryos.
(F and G) Percent Canoe intensity change 15 min post-wounding at BCJs at the wound edge (F) or at TCJs (G) in CanoeWT (n = 50 BCJs and 62 TCJs in 6 embryos) and in CanoeΔRA (n = 39 BCJs and 53 TCJs in 7 embryos).
(H and I) Myosin fluorescence at the wound edge (H), and maximum myosin accumulation at the wound edge (I) in dsRNA *canoe* (n = 5, black), CanoeWT (n = 6, blue), and CanoeΔRA (n = 7, red) embryos.
(D and H) Error bars, SEM.
(E–G and I) Error bars, SD; boxes, SEM; gray lines, mean. *p < 0.05, ***p < 0.001, Mann-Whitney U test (F and G) or Dunn's test (E and I).
See also Figures S4 and S5 and Video S3.

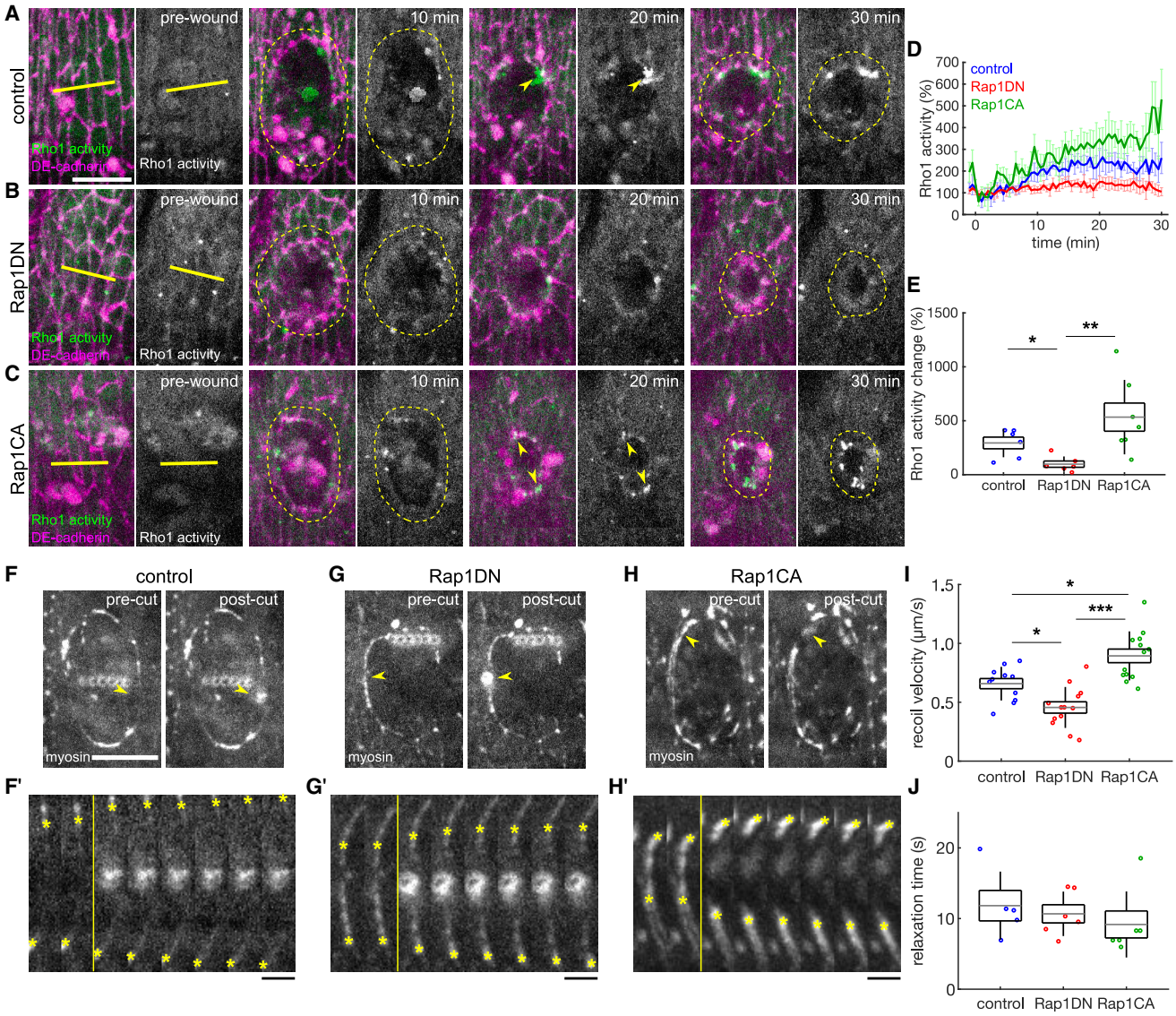

Figure 6. Rap1 regulates Rho1 activity and force generation at the wound edge

(A–C) Epidermal cells in wounded control (*daGal4* × *yw*, A), Rap1DN (*daGal4* × *UAS-Rap1DN*, B), and Rap1CA (*daGal4* × *UAS-Rap1CA*, C) embryos expressing DE-cadherin:tdTomato (magenta) and a single copy of the Rho1 activity sensor GFP:AnillinRBD (green and grayscale). Yellow lines denote wound sites, yellow dashed lines indicate the wound edge, and yellow arrowheads indicate Rho1 puncta. Anterior left, dorsal up. Scale bar, 15 μm.

(D and E) Rho1 sensor fluorescence at the wound edge relative to the time of wounding (D) and fold-change in Rho1 sensor at maximum intensity relative to the time of wounding (E) for control (n = 6, blue), Rap1DN (n = 6, red), and Rap1CA (n = 7, green) embryos.

(F–H) Epidermal cells in wounded embryos expressing Sqh:GFP prior to (left) and immediately after (right) severing of the wound edge cable, and kymographs of myosin in cable segments in control embryos (*daGal4* × *yw*, F and F′), Rap1DN (*daGal4* × *UAS-Rap1DN*, G and G′), and Rap1CA (*daGal4* × *UAS-Rap1CA*, H and H′). Yellow arrowheads indicate site of point ablation, yellow lines denote time of wounding, and yellow asterisks indicate the ends of the severed cable segment. Scale bars, 15 μm (F–H), 4 s (F′–H′).

(I and J) Initial retraction velocity (I) and relaxation time (J) after cable ablation in control (n = 11, blue), Rap1DN (n = 13, red), and Rap1CA (n = 13, green) embryos. (D) Error bars, SEM.

(E, I, and J) Error bars, SD; boxes, SEM; gray lines, mean. *p < 0.05, **p < 0.01, ***p < 0.001, Dunn's test.

See also Figure S6 and Videos S4 and S5.

Rap1 acts through the RhoGEF Ephexin to activate Rho1 and polarize myosin during wound closure

To establish how Rap1 regulates Rho1 activity and myosin polarity, we investigated the role that the Rho GEF Ephexin plays in embryonic wound healing. In *C. elegans*, Rap1 can activate RhoA through Ephexin.[55] In the dorsal thorax of *Drosophila* pupae, Ephexin localizes to the adherens junctions of interphase cells and the contractile cytokinetic ring of dividing cells, both sites of force generation and transmission.[56] To determine if Rap1 signals through Ephexin during wound healing, we used

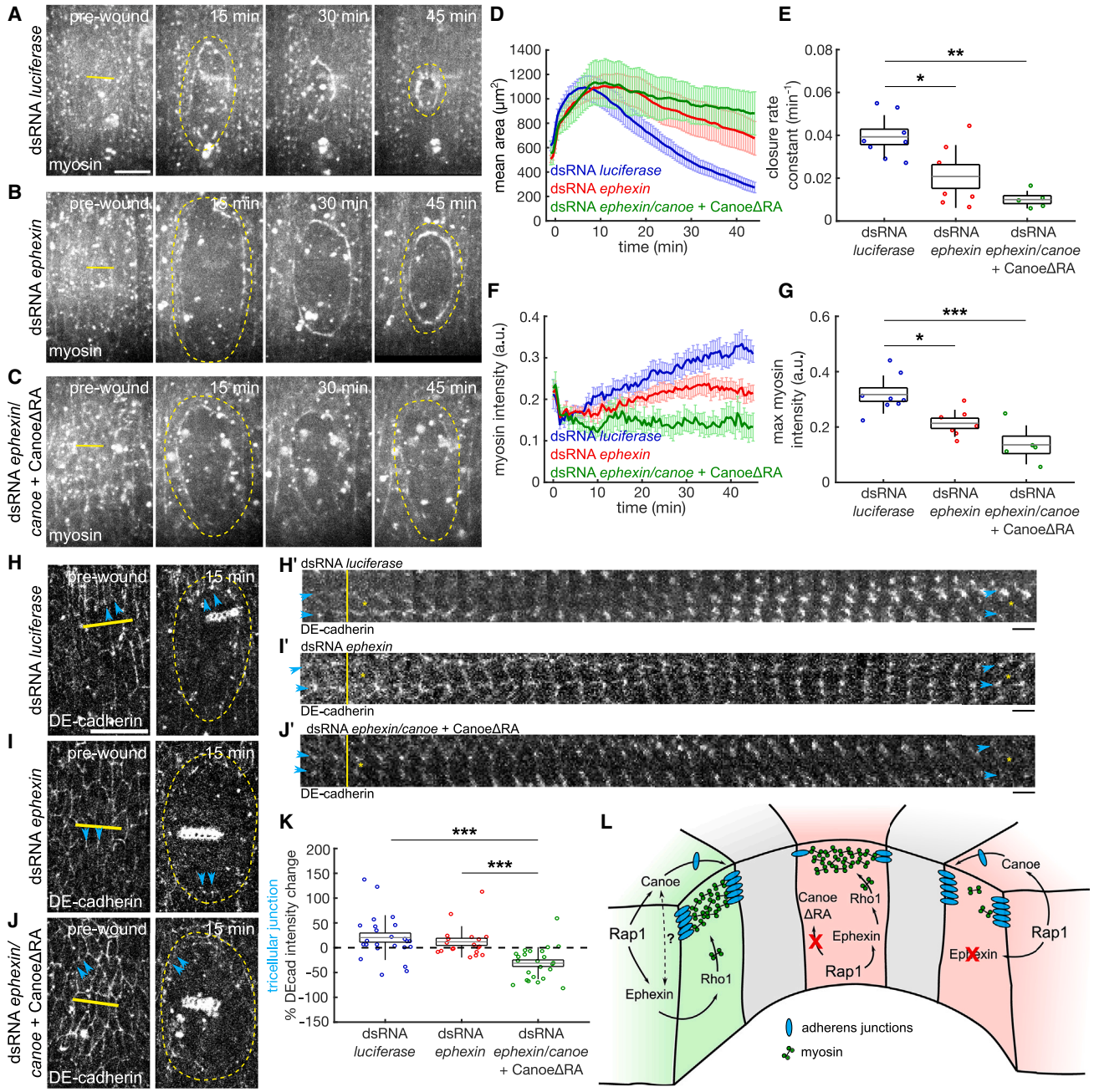

Figure 7. The Rho GEF Ephexin regulates myosin polarization during embryonic wound healing

(A–C) Epidermal cells in wounded embryos expressing Sqh:mCherry and injected with dsRNA against *luciferase* (*daGal4* × *yw*, A), dsRNA against *ephexin* (*daGal4* × *yw*, B), or dsRNA against *ephexin* and *canoe* and also expressing CanoeΔRA (*daGal4* × *UAS-Canoe* Δ *RA:Venus*, C). Yellow lines denote wound sites, yellow dashed lines indicate the wound edge. Anterior left, dorsal up. Scale bar, 15 μm.

(D–G) Wound area over time (D), wound closure rate constant (E), myosin fluorescence at the wound edge (F), and maximum myosin accumulation at the wound edge (G) in embryos injected with *luciferase* dsRNA (n = 8, blue), *ephexin* dsRNA (n = 7, red), or with *ephexin* dsRNA and *canoe* dsRNA and expressing CanoeΔRA (n = 5, green) embryos.

(H–J) Epidermal cells in wounded embryos expressing DE-cadherin:tdTomato and injected with dsRNA against *luciferase* (*daGal4* × *yw*, H), dsRNA against *ephexin* (*daGal4* × *yw*, I), or dsRNA against *ephexin* and *canoe* and also expressing CanoeΔRA (daGal4 × UAS-CanoeΔRA:Venus, J). Yellow lines denote wound sites and yellow dashed lines indicate the wound edge. Cyan arrowheads indicate TCJs flanking the BCJs shown in (H′)–(J′). Anterior left, dorsal up. Scale bar, 15 μm.

(H′–J′) Kymographs of a TCJ pair and connecting BCJ from embryos in (H)–(J). Yellow lines denote time of wounding and yellow asterisks show location of the wound relative. Scale bars, 30 s.

(K) Percent DE-cadherin intensity change 15 min post-wounding at TCJs at the wound edge in embryos injected with *luciferase* dsRNA (n = 17 TCJs in 3 embryos), *ephexin* dsRNA (n = 21 TCJs in 3 embryos), or with *ephexin* dsRNA and *canoe* dsRNA and expressing CanoeΔRA (n = 17 TCJs in 3 embryos).

(legend continued on next page)

the UAS-Gal4 system to simultaneously drive expression of Ephexin:YFP and either a control UAS construct or Rap1DN. We quantified the localization of Ephexin at the wound edge and found that in controls, Ephexin levels increased to a maximum of 3.2-fold with respect to initial levels (Figures S7A–S7C). Ephexin levels at the wound edge were 25% lower in Rap1DN embryos ($p = 0.022$; Figures S7B–S7D). Thus, Rap1 directs Ephexin polarization during embryonic wound healing.

To determine whether Ephexin contributes to the wound repair process, we knocked down Ephexin using dsRNA injected in syncytial embryos expressing myosin:mCherry. dsRNA against *ephexin* slowed wound repair by 47% relative to embryos injected with dsRNA against *luciferase* as a control ($p = 0.037$; Figures 7A, 7B, 7D, and 7E; Video S6), indicating that Ephexin is necessary for rapid wound closure. To investigate whether Ephexin contributes to wound healing in parallel to Rap1-Canoe signaling, we quantified the dynamics of wound repair in embryos injected with dsRNA against both *ephexin* and *canoe* and expressing CanoeΔRA (Figures 7A–7C). The combined disruption of Ephexin and Rap1-Canoe signaling slowed down wound closure by an additional 52% with respect to the Ephexin knockdown alone (Figures 7D and 7E), suggesting that Ephexin contributes to wound repair through mechanisms at least partially independent of the Rap1-Canoe regulation of adherens junction remodeling.

To investigate whether Ephexin was involved in Rho1-myosin activation during wound healing, we quantified Rho1 activity and myosin polarization during wound repair in *ephexin* dsRNA embryos. We found that Ephexin knockdown abolished Rho1 activity at the leading edge throughout wound closure ($p = 0.022$ relative to controls; Figures S7E–S7H). Consistently, *ephexin* dsRNA reduced the maximum myosin accumulation at the wound edge by 33% relative to controls ($p = 0.024$; Figures 7A, 7B, 7F, and 7G). The addition of *canoe* dsRNA and CanoeΔRA expression resulted in an additional modest decrease in myosin localization to the wound edge, suggesting a potential synergistic effect between Ephexin and Canoe (Figures 7A–7C, 7F, and 7G). Notably, Ephexin knockdown did not affect DE-cadherin dynamics at TCJs significantly: DE-cadherin levels at TCJs increased by 20% ± 9% in controls and by 12% ± 7% in *ephexin* dsRNA embryos (Figures 7H, 7I, and 7K). The combined effects of Ephexin knockdown and the disruption of Rap1-Canoe signaling with CanoeΔRA significantly affected the reinforcement of TCJs, in which DE-cadherin levels decreased by 31% ± 7% (Figures 7H–7K). Our results indicate that Ephexin acts downstream of Rap1 to regulate Rho1 activity and myosin accumulation at the wound edge without effects on adherens junction dynamics, thus facilitating rapid wound healing.

DISCUSSION

We demonstrate a crucial role for Rap1 in driving collective cell migration to heal epidermal wounds. Rap1 plays a dual role in embryonic wound repair in which (1) Rap1 drives adherens junction reinforcement at former TCJs via interactions with Canoe, and (2) Rap1 promotes myosin polarization to the wound edge via activation of Rho1 through Ephexin (Figure 7L). Both Rap1 functions are independently controlled and required to drive rapid wound repair.

The signals that drive Rap1 activation and TCJ assembly around the wound are unclear. Rap1 accumulates and is active at the wound edge shortly following wounding. The redistribution and activation of Rap1 occurs in parallel with the internalization of adherens junctions from the wound edge and the accumulation of adherens junction components at TCJs. DE-cadherin endocytosis during wound healing occurs in a Src-dependent manner.[22] Notably, E-cadherin endocytosis can drive Src-dependent Rap1 activation in mammalian cells in culture,[57] suggesting that the internalization of adherens junctions from the wound edge could promote Rap1 activation. In turn, we found that Rap1 and Canoe are required to drive DE-cadherin localization to TCJs. Furthermore, the recycling factor Rab11 is a binding partner of Rap1,[58] suggesting that recycling of endocytosed material may play a key role in TCJ assembly during wound repair.

Our results indicate that assembly of TCJs is necessary for rapid wound healing. TCJs have been proposed to be sites of actomyosin cable formation.[20] TCJs could also be important sites for anchoring the actomyosin cable and enabling force transmission to neighboring cells. We found robust myosin polarization to the wound edge and force-dependent myosin dynamics when TCJs were disrupted by interfering with Rap1-Canoe binding. In contrast, Ephexin knockdown reduced myosin polarization, and the additional disruption of Rap1-Canoe binding caused an enhancement of the myosin defect. Canoe/Afadin can interact with Eph receptors upstream of Ephexin signaling,[59] suggesting that Canoe at TCJs might stabilize Eph-Ephexin signaling and thus contribute to cytoskeletal assembly at the wound edge. Alternatively, reinforcement of TCJs could affect cell-matrix adhesion, an understudied aspect of embryonic wound repair.[60] The cross-talk between adherens junctions and cell-matrix adhesions is well known[61] and in the *Drosophila* embryo reducing cell-cell adhesion, similar to the BCJ internalization during wound healing, can upregulate cell-matrix adhesion.[62] Additionally, a local increase in force on cadherins, which likely occurs at the TCJs during wound repair, can reinforce cell-ECM adhesion through Rho-dependent signaling.[63]

Our data indicate that both the assembly of TCJs and the actomyosin cable are necessary for optimal wound repair. Rapid wound healing requires actomyosin polarization to the wound edge,[17] but we show that actomyosin polarization is not sufficient for rapid wound closure in the absence of TCJ assembly. Similarly, although E-cadherin endocytosis is required for assembly of the actomyosin cable,[19,20] it is not sufficient to drive cable assembly or rapid wound healing in the absence of Rho1 activation. Notably, our results indicate that Rap1 plays

(L) Schematic showing how Rap1 contributes to the molecular rearrangements required for rapid wound closure.
(D and F) Error bars, SEM.
(E, G, and K) Error bars, SD; boxes, SEM; gray lines, mean. *$p < 0.05$, **$p < 0.01$, ***$p < 0.001$, Dunn's test.
See also Figure S7 and Video S6.

independent roles in guiding both junctional and cytoskeletal rearrangements (Figure 7L). Consistent with this, Rap1-Canoe signaling regulates the planar polarity of junctional proteins in developing *Drosophila* embryos, while Rap1 has Canoe-independent roles controlling apical constriction and the recruitment of junctional proteins to adherens junctions.[64]

We demonstrate Rho1 activation that depends on Rap1 and Ephexin. Rho1 activity emerges in a heterogeneous pattern of puncta that may reflect the initial myosin heterogeneity upon wounding.[14] Rap1 can regulate cytoskeletal organization through Rho-family GTPases, both *in vitro*[28,65,66] and *in vivo*.[55] In many systems, Rap1 inhibits Rho1/RhoA signaling by activating Rac1 and Cdc42. However, disrupting Rac signaling in *Drosophila* embryonic wound repair does not cause major defects in cytoskeletal polarization to the wound edge,[5,67] and Cdc42 mainly regulates protrusive activity.[5,17] Rap1 can also activate Rho1/RhoA via the integrin-binding protein and Rap1 effector Talin, which promotes Ephexin phosphorylation by Src.[55] Rap1 recruits Talin to integrin-based adhesions that link cells to the extracellular matrix.[68] While the role of integrin-based adhesions in embryonic wound healing is unknown, integrins are necessary for *Drosophila* dorsal closure,[69] a process reminiscent of wound healing. Furthermore, apical integrin-based adhesion is necessary for the coordinated cell movements that drive axis elongation in *Drosophila*.[70] Whether integrin-based adhesions act as sites of Rap1-induced Rho1 activation remains to be determined.

How is Rap1 activated at the onset of wound closure? Different signals at the wound edge may activate Rap1 GEFs, potentially leading to the polarized activation of Rap1 around the wound. PDZ-GEF (Dizzy) activates Rap1 to regulate cell-cell adhesion and actin protrusion during *Drosophila* border cell migration.[30] Additionally, PDZ-GEF controls Canoe localization to TCJs during polarity establishment in early fly embryos[29] and regulates cell shape and plasticity in epithelial cells.[71] The GEF Epac is commonly studied as an activator of Rap1 in endothelial cell-cell adhesion,[72] and Epac is sensitive to ROS,[24] which is an important cue for wound edge polarization.[22] *In vitro*, C3G, a general Ras-family GEF that specifically acts on Rap1 in *Drosophila*,[73] is activated by cell stretching[25] and is required for Abl-dependent actin remodeling.[74] Notably, both cell stretching and Abl contribute to cytoskeletal dynamics during embryonic wound closure.[14,18] The development of tools to locally manipulate the mechanochemical signals implicated in the wound response will shed light on the mechanisms of Rap1 activation that mediate rapid wound healing.

STAR★METHODS

Detailed methods are provided in the online version of this paper and include the following:

SUPPLEMENTAL INFORMATION

Supplemental information can be found online at https://doi.org/10.1016/j.cub.2023.05.009.

ACKNOWLEDGMENTS

We wish to acknowledge this land on which the University of Toronto operates. For thousands of years, it has been the traditional land of the Huron-Wendat, the Seneca, and the Mississaugas of the Credit. Today, this meeting place is still the home to many Indigenous people from across Turtle Island and we are grateful to have the opportunity to work on this land. We are particularly thankful to Mark Peifer for reagents, discussion, and feedback on the manuscript. We are grateful to Guy Tanentzapf, Ulli Tepass, and Jennifer Zallen for reagents. We thank Ana Maria Carmo, Michelle Ly, and Gordana Scepanovic for feedback on the manuscript. We used resources from the Drosophila Genomics Resource Center (NIH grant 2P40OD010949). Flybase provided important information for this study. This work was funded by grants from the Canadian Institutes of Health Research (156279) and the Canada Foundation for Innovation (30279) to R.F.-G. and from the National Science Foundation (1738757) to J.A.M. K.E.R. was supported by postdoctoral fellowships from the Canadian Institutes of Health Research and the Ted Rogers Centre for Heart Research. R.F.-G. is the Canada Research Chair in Quantitative Cell Biology and Morphogenesis.

AUTHOR CONTRIBUTIONS

Conceptualization, methodology, software, formal analysis, investigation, writing, and visualization, K.E.R.; methodology and resources, Y.C.; methodology, resources, writing – review & editing, J.A.M.; conceptualization, methodology, software, resources, writing, supervision, project administration, and funding acquisition, R.F.-G.

DECLARATION OF INTERESTS

The authors declare no competing interests.

INCLUSION AND DIVERSITY

We support inclusive, diverse, and equitable conduct of research.

Received: October 5, 2022
Revised: March 16, 2023
Accepted: May 4, 2023
Published: May 26, 2023

REFERENCES

1. Friedl, P., and Gilmour, D. (2009). Collective cell migration in morphogenesis, regeneration and cancer. Nat. Rev. Mol. Cell Biol. *10*, 445–457. https://doi.org/10.1038/nrm2720.
2. Stock, J., and Pauli, A. (2021). Self-organized cell migration across scales - from single cell movement to tissue formation. Development *148*, https://doi.org/10.1242/dev.191767.

3. Jacinto, A., Wood, W., Balayo, T., Turmaine, M., Martinez-Arias, A., and Martin, P. (2000). Dynamic actin-based epithelial adhesion and cell matching during Drosophila dorsal closure. Curr. Biol. *10*, 1420–1426.
4. Kiehart, D.P., Galbraith, C.G., Edwards, K.A., Rickoll, W.L., and Montague, R.A. (2000). Multiple forces contribute to cell sheet morphogenesis for dorsal closure in Drosophila. J. Cell Biol. *149*, 471–490.
5. Wood, W., Jacinto, A., Grose, R., Woolner, S., Gale, J., Wilson, C., and Martin, P. (2002). Wound healing recapitulates morphogenesis in Drosophila embryos. Nat. Cell Biol. *4*, 907–912. https://doi.org/10.1038/ncb875.
6. Davidson, L.A., Hoffstrom, B.G., Keller, R., and DeSimone, D.W. (2002). Mesendoderm extension and mantle closure in Xenopus laevis gastrulation: combined roles for integrin $\alpha5\beta1$, fibronectin, and tissue geometry. Dev. Biol. *242*, 109–129. https://doi.org/10.1006/dbio.2002.0537.
7. Montero, J.-A., Kilian, B., Chan, J., Bayliss, P.E., and Heisenberg, C.-P. (2003). Phosphoinositide 3-kinase is required for process outgrowth and cell polarization of gastrulating mesendodermal cells. Curr. Biol. *13*, 1279–1289. https://doi.org/10.1016/S0960-9822(03)00505-0.
8. Kuriyama, S., Theveneau, E., Benedetto, A., Parsons, M., Tanaka, M., Charras, G., Kabla, A., and Mayor, R. (2014). In vivo collective cell migration requires an LPAR2-dependent increase in tissue fluidity. J. Cell Biol. *206*, 113–127. https://doi.org/10.1083/jcb.201402093.
9. Friedl, P., and Wolf, K. (2003). Tumour-cell invasion and migration: diversity and escape mechanisms. Nat. Rev. Cancer *3*, 362–374. https://doi.org/10.1038/nrc1075.
10. Zhang, Y., and Weinberg, R.A. (2018). Epithelial-to-mesenchymal transition in cancer: complexity and opportunities. Front. Med. *12*, 361–373. https://doi.org/10.1007/s11684-018-0656-6.
11. Martin, P., and Lewis, J. (1992). Actin cables and epidermal movement in embryonic wound healing. Nature *360*, 179–183. https://doi.org/10.1038/360179a0.
12. McCluskey, J., and Martin, P. (1995). Analysis of the tissue movements of embryonic wound healing–DiI studies in the limb bud stage mouse embryo. Dev. Biol. *170*, 102–114. https://doi.org/10.1006/dbio.1995.1199.
13. Davidson, L.A., Ezin, A.M., and Keller, R. (2002). Embryonic wound healing by apical contraction and ingression in Xenopus laevis. Cell Motil. Cytoskelet. *53*, 163–176. https://doi.org/10.1002/cm.10070.
14. Zulueta-Coarasa, T., and Fernandez-Gonzalez, R. (2018). Dynamic force patterns promote collective cell movements during embryonic wound repair. Nat. Phys. *14*, 750–758. https://doi.org/10.1038/s41567-018-0111-2.
15. Rothenberg, K.E., and Fernandez-Gonzalez, R. (2019). Forceful closure: cytoskeletal networks in embryonic wound repair. Mol. Biol. Cell *30*, 1353–1358. https://doi.org/10.1091/mbc.E18-04-0248.
16. Brock, J., Midwinter, K., Lewis, J., and Martin, P. (1996). Healing of incisional wounds in the embryonic chick wing bud: characterization of the actin purse-string and demonstration of a requirement for Rho activation. J. Cell Biol. *135*, 1097–1107.
17. Abreu-Blanco, M.T., Verboon, J.M., Liu, R., Watts, J.J., and Parkhurst, S.M. (2012). Drosophila embryos close epithelial wounds using a combination of cellular protrusions and an actomyosin purse string. J. Cell Sci. *125*, 5984–5997. https://doi.org/10.1242/jcs.109066.
18. Zulueta-Coarasa, T., Tamada, M., Lee, E.J., and Fernandez-Gonzalez, R. (2014). Automated multidimensional image analysis reveals a role for Abl in embryonic wound repair. Development *141*, 2901–2911. https://doi.org/10.1242/dev.106898.
19. Hunter, M.V., Lee, D.M., Harris, T.J., and Fernandez-Gonzalez, R. (2015). Polarized E-cadherin endocytosis directs actomyosin remodeling during embryonic wound repair. J. Cell Biol. *210*, 801–816. https://doi.org/10.1083/jcb.201501076.
20. Matsubayashi, Y., Coulson-Gilmer, C., and Millard, T.H. (2015). Endocytosis-dependent coordination of multiple actin regulators is required for wound healing. J. Cell Biol. *210*, 419–433. https://doi.org/10.1083/jcb.201411037.
21. Razzell, W., Evans, I.R., Martin, P., and Wood, W. (2013). Calcium flashes orchestrate the wound inflammatory response through DUOX activation and hydrogen peroxide release. Curr. Biol. *23*, 424–429. https://doi.org/10.1016/j.cub.2013.01.058.
22. Hunter, M.V., Willoughby, P.M., Bruce, A.E.E., and Fernandez-Gonzalez, R. (2018). Oxidative stress orchestrates cell polarity to promote embryonic wound healing. Dev. Cell *47*, 377–387.e4. https://doi.org/10.1016/j.devcel.2018.10.013.
23. Zechini, L., Amato, C., Scopelliti, A., and Wood, W. (2022). Piezo acts as a molecular brake on wound closure to ensure effective inflammation and maintenance of epithelial integrity. Curr. Biol. *32*, 3584–3592.e4. https://doi.org/10.1016/j.cub.2022.06.041.
24. Moon, E.Y., Lee, J.H., Lee, J.W., Song, J.H., and Pyo, S. (2011). ROS/Epac1-mediated Rap1/NF-kappaB activation is required for the expression of BAFF in Raw264.7 murine macrophages. Cell. Signal. *23*, 1479–1488. https://doi.org/10.1016/j.cellsig.2011.05.001.
25. Tamada, M., Sheetz, M.P., and Sawada, Y. (2004). Activation of a signaling cascade by cytoskeleton stretch. Dev. Cell *7*, 709–718. https://doi.org/10.1016/j.devcel.2004.08.021.
26. Knox, A.L., and Brown, N.H. (2002). Rap1 GTPase regulation of adherens junction positioning and cell adhesion. Science *295*, 1285–1288. https://doi.org/10.1126/science.1067549.
27. Spahn, P., Ott, A., and Reuter, R. (2012). The PDZ-GEF protein Dizzy regulates the establishment of adherens junctions required for ventral furrow formation in Drosophila. J. Cell Sci. *125*, 3801–3812. https://doi.org/10.1242/jcs.101196.
28. Ando, K., Fukuhara, S., Moriya, T., Obara, Y., Nakahata, N., and Mochizuki, N. (2013). Rap1 potentiates endothelial cell junctions by spatially controlling myosin II activity and actin organization. J. Cell Biol. *202*, 901–916. https://doi.org/10.1083/jcb.201301115.
29. Bonello, T.T., Perez-Vale, K.Z., Sumigray, K.D., and Peifer, M. (2018). Rap1 acts via multiple mechanisms to position Canoe and adherens junctions and mediate apical-basal polarity establishment. Development *145*, dev157941, https://doi.org/10.1242/dev.157941.
30. Sawant, K., Chen, Y., Kotian, N., Preuss, K.M., and McDonald, J.A. (2018). Rap1 GTPase promotes coordinated collective cell migration in vivo. Mol. Biol. Cell *29*, 2656–2673. https://doi.org/10.1091/mbc.E17-12-0752.
31. Perez-Vale, K.Z., Yow, K.D., Johnson, R.I., Byrnes, A.E., Finegan, T.M., Slep, K.C., and Peifer, M. (2021). Multivalent interactions make adherens junction-cytoskeletal linkage robust during morphogenesis. J. Cell Biol. *220*, e202104087, https://doi.org/10.1083/jcb.202104087.
32. Messer, C.L., and McDonald, J.A. (2022). Rap1 promotes epithelial integrity and cell viability in a growing tissue. Preprint at bioRxiv. https://doi.org/10.1101/2022.10.21.513265.
33. Smutny, M., Cox, H.L., Leerberg, J.M., Kovacs, E.M., Conti, M.A., Ferguson, C., Hamilton, N.A., Parton, R.G., Adelstein, R.S., and Yap, A.S. (2010). Myosin II isoforms identify distinct functional modules that support integrity of the epithelial zonula adherens. Nat. Cell Biol. *12*, 696–702. https://doi.org/10.1038/ncb2072.
34. Boettner, B., Harjes, P., Ishimaru, S., Heke, M., Fan, H.Q., Qin, Y., Van Aelst, L., and Gaul, U. (2003). The AF-6 homolog canoe acts as a Rap1 effector during dorsal closure of the Drosophila embryo. Genetics *165*, 159–169.
35. Yu, H.H., and Zallen, J.A. (2020). Abl and Canoe/Afadin mediate mechanotransduction at tricellular junctions. Science *370*, eaba5528, https://doi.org/10.1126/science.aba5528.
36. Zhang, Y.L., Wang, R.C., Cheng, K., Ring, B.Z., and Su, L. (2017). Roles of Rap1 signaling in tumor cell migration and invasion. Cancer Biol. Med. *14*, 90–99. https://doi.org/10.20892/j.issn.2095-3941.2016.0086.
37. Shah, S., Brock, E.J., Ji, K., and Mattingly, R.R. (2019). Ras and Rap1: a tale of two GTPases. Semin. Cancer Biol. *54*, 29–39. https://doi.org/10.1016/j.semcancer.2018.03.005.

38. Looi, C.K., Hii, L.W., Ngai, S.C., Leong, C.O., and Mai, C.W. (2020). The role of Ras-associated Protein 1 (Rap1) in cancer: bad actor or good player? Biomedicines *8*, 334, https://doi.org/10.3390/biomedicines8090334.

39. Huang, J., Zhou, W., Dong, W., Watson, A.M., and Hong, Y. (2009). From the cover: directed, efficient, and versatile modifications of the Drosophila genome by genomic engineering. Proc. Natl. Acad. Sci. USA *106*, 8284–8289. https://doi.org/10.1073/pnas.0900641106.

40. Nagarkar-Jaiswal, S., Lee, P.-T., Campbell, M.E., Chen, K., Anguiano-Zarate, S., Gutierrez, M.C., Busby, T., Lin, W.-W., He, Y., Schulze, K.L., et al. (2015). A library of MiMICs allows tagging of genes and reversible, spatial and temporal knockdown of proteins in Drosophila. eLife *4*, e05338, https://doi.org/10.7554/eLife.05338.

41. Lowe, N., Rees, J.S., Roote, J., Ryder, E., Armean, I.M., Johnson, G., Drummond, E., Spriggs, H., Drummond, J., Magbanua, J.P., et al. (2014). Analysis of the expression patterns, subcellular localisations and interaction partners of Drosophila proteins using a pigP protein trap library. Development *141*, 3994–4005. https://doi.org/10.1242/dev.111054.

42. Lye, C.M., Naylor, H.W., and Sanson, B. (2014). Subcellular localisations of the CPTI collection of YFP-tagged proteins in Drosophila embryos. Development *141*, 4006–4017. https://doi.org/10.1242/dev.111310.

43. Schneider, I. (1972). Cell lines derived from late embryonic stages of Drosophila melanogaster. J. Embryol. Exp. Morphol. *27*, 353–365.

44. Dupuy, A.G., L'Hoste, S., Cherfils, J., Camonis, J., Gaudriault, G., and de Gunzburg, J. (2005). Novel Rap1 dominant-negative mutants interfere selectively with C3G and EPAC. Oncogene *24*, 4509–4520. https://doi.org/10.1038/sj.onc.1208647.

45. Brand, A.H., and Perrimon, N. (1993). Targeted gene expression as a means of altering cell fates and generating dominant phenotypes. Development *118*, 401–415.

46. Royou, A., Field, C., Sisson, J.C., Sullivan, W., and Karess, R. (2004). Reassessing the role and dynamics of nonmuscle myosin II during furrow formation in early Drosophila embryos. Mol. Biol. Cell *15*, 838–850. https://doi.org/10.1091/mbc.e03-06-0440.

47. Buszczak, M., Paterno, S., Lighthouse, D., Bachman, J., Planck, J., Owen, S., Skora, A.D., Nystul, T.G., Ohlstein, B., Allen, A., et al. (2007). The carnegie protein trap library: a versatile tool for Drosophila developmental studies. Genetics *175*, 1505–1531. https://doi.org/10.1534/genetics.106.065961.

48. Staller, M.V., Yan, D., Randklev, S., Bragdon, M.D., Wunderlich, Z.B., Tao, R., Perkins, L.A., Depace, A.H., and Perrimon, N. (2013). Depleting gene activities in early Drosophila embryos with the "maternal-Gal4-shRNA" system. Genetics *193*, 51–61. https://doi.org/10.1534/genetics.112.144915.

49. Martin, A.C., Kaschube, M., and Wieschaus, E.F. (2009). Pulsed contractions of an actin-myosin network drive apical constriction. Nature *457*, 495–499. https://doi.org/10.1038/nature07522.

50. Munjal, A., Philippe, J.M., Munro, E., and Lecuit, T. (2015). A self-organized biomechanical network drives shape changes during tissue morphogenesis. Nature *524*, 351–355. https://doi.org/10.1038/nature14603.

51. Barrett, K., Leptin, M., and Settleman, J. (1997). The Rho GTPase and a putative RhoGEF mediate a signaling pathway for the cell shape changes in Drosophila gastrulation. Cell *91*, 905–915. https://doi.org/10.1016/S0092-8674(00)80482-1.

52. Abreu-Blanco, M.T., Verboon, J.M., and Parkhurst, S.M. (2014). Coordination of Rho family GTPase activities to orchestrate cytoskeleton responses during cell wound repair. Curr. Biol. *24*, 144–155. https://doi.org/10.1016/j.cub.2013.11.048.

53. Simões, M., Blankenship, J.T., Weitz, O., Farrell, D.L., Tamada, M., Fernandez-Gonzalez, R., and Zallen, J.A. (2010). Rho-kinase directs Bazooka/Par-3 planar polarity during Drosophila axis elongation. Dev. Cell *19*, 377–388. https://doi.org/10.1016/j.devcel.2010.08.011.

54. Zulueta-Coarasa, T., and Fernandez-Gonzalez, R. (2015). Laser ablation to investigate cell and tissue mechanics in vivo. In Integrative Mechanobiology: Micro- and Nano- Techniques in Cell Mechanobiology, C.A. Simmons, D.-H. Kim, and Y. Sun, eds. (Cambridge University Press), pp. 128–147. https://doi.org/10.1017/CBO9781139939751.009.

55. Sakai, Y., Tsunekawa, M., Ohta, K., Shimizu, T., Pastuhov, S., Hanafusa, H., Hisamoto, N., and Matsumoto, K. (2021). The integrin signaling network promotes axon regeneration via the Src–Ephexin–RhoA GTPase signaling axis. J. Neurosci. *41*, 4754–4767. https://doi.org/10.1523/JNEUROSCI.2456-20.2021.

56. Pietro, F. di, Osswald, M., De Las Heras, J.M.D. las, Cristo, I., López-Gay, J., Wang, Z., Pelletier, S., Gaugué, I., Leroy, A., Martin, C., et al. (2023). Systematic analysis of RhoGEF/GAP localizations uncovers regulators of mechanosensing and junction formation during epithelial cell division. Curr. Biol. *33*, 858–874.e7. https://doi.org/10.1016/j.cub.2023.01.028.

57. Balzac, F., Avolio, M., Degani, S., Kaverina, I., Torti, M., Silengo, L., Small, J.V., and Retta, S.F. (2005). E-cadherin endocytosis regulates the activity of Rap1: a traffic light GTPase at the crossroads between cadherin and integrin function. J. Cell Sci. *118*, 4765–4783. https://doi.org/10.1242/jcs.02584.

58. Kim, Y.S., Fan, R., Lith, S.C., Dicke, A.-K., Drexler, H.C.A., Kremer, L., Kuempel-Rink, N., Hekking, L., Stehling, M., and Bedzhov, I. (2022). Rap1 controls epiblast morphogenesis in sync with the pluripotency states transition. Dev. Cell *57*, 1937–1956.e8. https://doi.org/10.1016/j.devcel.2022.07.011.

59. Buchert, M., Schneider, S., Meskenaite, V., Adams, M.T., Canaani, E., Baechi, T., Moelling, K., and Hovens, C.M. (1999). The Junction-associated protein AF-6 interacts and clusters with specific Eph receptor tyrosine kinases at specialized sites of cell–cell contact in the brain. J. Cell Biol. *144*, 361–371. https://doi.org/10.1083/jcb.144.2.361.

60. Ly, M., Schimmer, C., Hawkins, R., Rothenberg, K., and Fernandez-Gonzalez, R. (2023). Integrin-based adhesions promote cell-cell junction remodelling and cytoskeletal rearrangements to drive embryonic wound healing. Preprint at bioRxiv. https://doi.org/10.1101/2023.03.13.532433.

61. Mui, K.L., Chen, C.S., and Assoian, R.K. (2016). The mechanical regulation of integrin-cadherin crosstalk organizes cells, signaling and forces. J. Cell Sci. *129*, 1093–1100. https://doi.org/10.1242/jcs.183699.

62. Goodwin, K., Lostchuck, E.E., Cramb, K.M.L., Zulueta-Coarasa, T., Fernandez-Gonzalez, R., and Tanentzapf, G. (2017). Cell–cell and cell–extracellular matrix adhesions cooperate to organize actomyosin networks and maintain force transmission during dorsal closure. Mol. Biol. Cell *28*, 1301–1310. https://doi.org/10.1091/mbc.E17-01-0033.

63. Kong, X., Kapustka, A., Sullivan, B., Schwarz, G.J., and Leckband, D.E. (2022). Extracellular matrix regulates force transduction at VE-cadherin junctions. Mol. Biol. Cell *33*, ar95. https://doi.org/10.1091/mbc.E22-03-0075.

64. Perez-Vale, K.Z., Yow, K.D., Gurley, N.J., Greene, M., and Peifer, M. (2023). Rap1 regulates apical contractility to allow embryonic morphogenesis without tissue disruption and acts in part via Canoe-independent mechanisms. Mol. Biol. Cell *34*, ar7. https://doi.org/10.1091/mbc.E22-05-0176.

65. Miyata, M., Rikitake, Y., Takahashi, M., Nagamatsu, Y., Yamauchi, Y., Ogita, H., Hirata, K., and Takai, Y. (2009). Regulation by afadin of cyclical activation and inactivation of Rap1, Rac1, and RhoA small G proteins at leading edges of moving NIH3T3 cells. J. Biol. Chem. *284*, 24595–24609. https://doi.org/10.1074/jbc.M109.016436.

66. Birukova, A.A., Tian, X., Tian, Y., Higginbotham, K., and Birukov, K.G. (2013). Rap-afadin axis in control of Rho signaling and endothelial barrier recovery. Mol. Biol. Cell *24*, 2678–2688. https://doi.org/10.1091/mbc.E13-02-0098.

67. Verboon, J.M., and Parkhurst, S.M. (2015). Rho family GTPase functions in Drosophila epithelial wound repair. Small GTPases *6*, 28–35. https://doi.org/10.4161/21541248.2014.982415.

68. Camp, D., Haage, A., Solianova, V., Castle, W.M., Xu, Q.A., Lostchuck, E., Goult, B.T., and Tanentzapf, G. (2018). Direct binding of Talin to Rap1 is required for cell–ECM adhesion in Drosophila. J. Cell Sci. *131*, jcs225144. https://doi.org/10.1242/jcs.225144.

69. Goodwin, K., Ellis, S.J., Lostchuck, E., Zulueta-Coarasa, T., Fernandez-Gonzalez, R., and Tanentzapf, G. (2016). Basal cell-extracellular matrix adhesion regulates force transmission during tissue morphogenesis. Dev. Cell *39*, 611–625. https://doi.org/10.1016/j.devcel.2016.11.003.

70. Münster, S., Jain, A., Mietke, A., Pavlopoulos, A., Grill, S.W., and Tomancak, P. (2019). Attachment of the blastoderm to the vitelline envelope affects gastrulation of insects. Nature *568*, 395–399. https://doi.org/10.1038/s41586-019-1044-3.

71. Boettner, B., and Van Aelst, L. (2007). The Rap GTPase activator Drosophila PDZ-GEF regulates cell shape in epithelial migration and morphogenesis. Mol. Cell. Biol. *27*, 7966–7980. https://doi.org/10.1128/MCB.01275-07.

72. Pannekoek, W.J., van Dijk, J.J., Chan, O.Y., Huveneers, S., Linnemann, J.R., Spanjaard, E., Brouwer, P.M., van der Meer, A.J., Zwartkruis, F.J., Rehmann, H., et al. (2011). Epac1 and PDZ-GEF cooperate in Rap1 mediated endothelial junction control. Cell. Signal. *23*, 2056–2064. https://doi.org/10.1016/j.cellsig.2011.07.022.

73. Shirinian, M., Popovic, M., Grabbe, C., Varshney, G., Hugosson, F., Bos, H., Rehmann, H., and Palmer, R.H. (2010). The Rap1 guanine nucleotide exchange factor C3G is required for preservation of larval muscle integrity in Drosophila melanogaster. PLoS One *5*, e9403, https://doi.org/10.1371/journal.pone.0009403.

74. Radha, V., Rajanna, A., Mitra, A., Rangaraj, N., and Swarup, G. (2007). C3G is required for c-Abl-induced filopodia and its overexpression promotes filopodia formation. Exp. Cell Res. *313*, 2476–2492. https://doi.org/10.1016/j.yexcr.2007.03.019.

75. Frank, C.A., Pielage, J., and Davis, G.W. (2009). A presynaptic homeostatic signaling system composed of the Eph receptor, ephexin, Cdc42, and CaV2.1 calcium channels. Neuron *61*, 556–569. https://doi.org/10.1016/j.neuron.2008.12.028.

76. Ellis, S.J., Goult, B.T., Fairchild, M.J., Harris, N.J., Long, J., Lobo, P., Czerniecki, S., Van Petegem, F., Schöck, F., Peifer, M., et al. (2013). Talin autoinhibition is required for morphogenesis. Curr. Biol. *23*, 1825–1833. https://doi.org/10.1016/j.cub.2013.07.054.

77. Perkins, L.A., Holderbaum, L., Tao, R., Hu, Y., Sopko, R., McCall, K., Yang-Zhou, D., Flockhart, I., Binari, R., Shim, H.-S., et al. (2015). The transgenic RNAi Project at Harvard Medical School: resources and validation. Genetics *201*, 843–852. https://doi.org/10.1534/genetics.115.180208.

78. Satoh, A.K., O'Tousa, J.E., Ozaki, K., and Ready, D.F. (2005). Rab11 mediates post-Golgi trafficking of rhodopsin to the photosensitive apical membrane of Drosophila photoreceptors. Development *132*, 1487–1497. https://doi.org/10.1242/dev.01704.

79. Perrin, L., Bloyer, S., Ferraz, C., Agrawal, N., Sinha, P., and Dura, J.M. (2003). The leucine zipper motif of the Drosophila AF10 homologue can inhibit PRE-mediated repression: implications for leukemogenic activity of human MLL-AF10 fusions. Mol. Cell. Biol. *23*, 119–130. https://doi.org/10.1128/MCB.23.1.119-130.2003.

80. Lee, T., and Luo, L. (1999). Mosaic analysis with a repressible cell marker for studies of gene function in neuronal morphogenesis. Neuron *22*, 451–461. https://doi.org/10.1016/s0896-6273(00)80701-1.

81. Schindelin, J., Arganda-Carreras, I., Frise, E., Kaynig, V., Longair, M., Pietzsch, T., Preibisch, S., Rueden, C., Saalfeld, S., Schmid, B., et al. (2012). Fiji: an open-source platform for biological-image analysis. Nat. Methods *9*, 676–682. https://doi.org/10.1038/nmeth.2019.

82. Fernandez-Gonzalez, R., and Zallen, J.A. (2011). Oscillatory behaviors and hierarchical assembly of contractile structures in intercalating cells. Phys. Biol. *8*, 045005. https://doi.org/10.1088/1478-3975/8/4/045005.

83. Fernandez-Gonzalez, R., Balaghi, N., Wang, K., Hawkins, R., Rothenberg, K., McFaul, C., Schimmer, C., Ly, M., do Carmo, A.M., Scepanovic, G., et al. (2022). PyJAMAS: open-source, multimodal segmentation and analysis of microscopy images. Bioinformatics *38*, 594–596. https://doi.org/10.1093/bioinformatics/btab589.

84. Oda, H., and Tsukita, S. (2001). Real-time imaging of cell-cell adherens junctions reveals that Drosophila mesoderm invagination begins with two phases of apical constriction of cells. J. Cell Sci. *114*, 493–501. https://doi.org/10.1242/jcs.114.3.493.

85. Gibson, D.G., Young, L., Chuang, R.Y., Venter, J.C., Hutchison, C.A., 3rd, and Smith, H.O. (2009). Enzymatic assembly of DNA molecules up to several hundred kilobases. Nat. Methods *6*, 343–345. https://doi.org/10.1038/nmeth.1318.

86. Scepanovic, G., Florea, A., and Fernandez-Gonzalez, R. (2021). Multiscale in vivo imaging of collective cell migration in Drosophila embryos. Methods Mol. Biol. *2179*, 199–224. https://doi.org/10.1007/978-1-0716-0779-4_17.

87. Herbert, S., Valon, L., Mancini, L., Dray, N., Caldarelli, P., Gros, J., Esposito, E., Shorte, S.L., Bally-Cuif, L., Aulner, N., et al. (2021). LocalZProjector and DeProj: a toolbox for local 2D projection and accurate morphometrics of large 3D microscopy images. BMC Biol. *19*, 136. https://doi.org/10.1186/s12915-021-01037-w.

88. Kuntz, S.G., and Eisen, M.B. (2014). Drosophila embryogenesis scales uniformly across temperature in developmentally diverse species. PLoS Genet. *10*, e1004293. https://doi.org/10.1371/journal.pgen.1004293.

STAR★METHODS

KEY RESOURCES TABLE

REAGENT or RESOURCE	SOURCE	IDENTIFIER
Antibodies		
Rabbit anti-Canoe	Mark Peifer	N/A
Mouse anti-Discs large	Developmental Studies Hybridoma Bank	Cat#: 4F3 anti-discs large; RRID: AB_528203
Goat anti-Rabbit IgG (H+L) Alexa 488	Invitrogen	Cat #: A-11008; RRID: AB_143165
Goat anti-Mouse IgG (H+L) Alexa 568	Invitrogen	Cat #: A-11004; RRID: AB_2534072
Bacterial and virus strains		
NEB 5-alpha Competent *E. coli* (High Efficiency)	New England BioLabs	Cat #: C2987
Chemicals, peptides, and recombinant proteins		
Phusion High-Fidelity DNA Polymerase	Thermo Scientific	Cat #: F530
Gibson Assembly Cloning Kit	New England BioLabs	Cat #: E5510S
BamHI-HF	New England BioLabs	Cat #: R3136
PspXI	New England BioLabs	Cat #: R0656
QIAprep Spin Miniprep Kit	QIAGEN	Cat #: 27104
QIAGEN Plasmid *Plus* Midi Kit	QIAGEN	Cat #:12943
Zymoclean Gel DNA Recovery Kit	Zymo Research	Cat #: D4001
FuGENE HD Transfection Reagent	Promega	Cat #: E2311
MEGAscript T7 Transcription Kit	Invitrogen	Cat #: AM1334
Phenol-chloroform-isoamyl alcohol mixture 25:24:1	Sigma-Aldrich	Cat #: 77617
Choloroform	Caledon	Cat #: 3000-1-10
Halocarbon oil 27	Sigma-Aldrich	Cat #: H8773
Halocarbon oil 700	Sigma-Aldrich	Cat #: H8898
Heptane	Caledon	Cat #: 5400-1-10
Formaldehyde, 37% by Weight, Certified ACS	Fisher Scientific	Cat #: F79
PBS, tablet form	Sigma-Aldrich	Cat #: P4417
Triton X-100	Fisher Scientific	Cat #: BP151
Prolong Gold Antifade Mountant	Invitrogen	Cat #: P36930
Schneider's Drosophila Medium	Gibco	Cat #: 21720024
Fetal Bovine Serum, Heat-Inactivated	Gibco	Cat #: 12484028
Antibiotic/Antimycotic 100X	Gibco	Cat #: 15240062
Concanavalin A Type IV-S	Sigma-Aldrich	Cat #: C5275
Experimental models: Cell lines		
D. melanogaster: S2R+ cells	Drosophila Genomics Resource Center	Stock #: 150; RRID: CVCL_Z831
Experimental models: Organisms/strains		
endo-DE-cadherin:tdTomato	Bloomington Drosophila Stock Center[39]	BDSC: 58789
α-catenin:EGFP MiMIC	Bloomington Drosophila Stock Center[40]	BDSC: 59405
rap1-GFP:rap1	Bloomington Drosophila Stock Center[26]	BDSC:97118
endo-canoe:YFP	Kyoto Drosophila Stock Center[41,42]	Stock: 115111
UAS-GFP:canoeRAΔNLS (Rap1 sensor)	This study	N/A
sqh-sqh:GFP	Bloomington Drosophila Stock Center[46]	BDSC: 57144
zipper-zipper:GFP	Bloomington Drosophila Stock Center[47]	BDSC: 51564
ubi-GFP:anillinRBD	Munjal et al.[50]	https://doi.org/10.1038/nature14603
UAS-canoeWT:Venus	Zallen Lab	N/A
UAS-canoeΔRA:Venus	Zallen Lab	N/A
sqh-sqh:mCherry	Martin et al.[49]	https://doi.org/10.1038/nature07522
UAS-diaRBD:GFP	Bloomington Drosophila Stock Center[52]	BDSC: 52292

(*Continued on next page*)

Continued

REAGENT or RESOURCE	SOURCE	IDENTIFIER
sqh-GFP:rok^{K116A}	Simoes Simões et al.[53]	https://doi.org/10.1016/j.devcel.2010.08.011
UAS-ephexin:YFP	Frank et al.[75]	https://doi.org/10.1016/j.neuron.2008.12.028
UAS-rap1S17A (Rap1DN)	Ellis et al.[76]	https://doi.org/10.1016/j.cub.2013.07.054
UAS-rap1Q63E (Rap1CA)	Ellis et al.[76]	https://doi.org/10.1016/j.cub.2013.07.054
UAS-rap1-RNAi	Bloomington Drosophila Stock Center[77]	BDSC: 7328
UAS-canoe-RNAi	Bloomington Drosophila Stock Center[77]	BDSC: 33367
UAS-rho1N19	Bloomington Drosophila Stock Center[51]	BDSC: 7328
UAS-mCherry-RNAi	Bloomington Drosophila Stock Center[77]	BDSC: 35785
UAS-ECFP:Golgi	Bloomington Drosophila Stock Center[78]	BDSC: 42710
daughterless-Gal4	Perrin et al.[79]	https://doi.org/10.1128/MCB.23.1.119-130.2003
tubulin-Gal4	Lee and Luo[80]	https://doi.org/10.1016/s0896-6273(00)80701-1
yellow white	N/A	N/A
Oligonucleotides		
Rap1 activity sensor primers	This study	N/A
eGFP-fwd: 5'-AGCAGGCTCCGCGGCCGCATGGTGAGCAAGGGCGAG- 3'		
eGFP-rvs: 5'-ATGGTGAAGGGGCCCGGGCGCTTGTACAGCTCGTCCATGC- 3'		
RA1-fwd: 5'-GAGCTGTACAAGCGCCCGGGCCCCTTCACCATGTCACATG-3'		
RA1-rvs: 5'-GGGCGGATCAGAGCTCAGAAAGTTTAGATCTGTCTGCTCG-3'		
RA2-fwd: 5'-CGAGCAGACAGATCTAAACTTTCTGAGCTCTGATCCGCCC-3'		
RA2-rvs: 5'-TCGAGGTCGACTCTAGCTTACACATGGAACATGATGGAGC-3'		
Vector1-fwd: 5'-GCTCCATCATGTTCCATGTGTAAGCTAGAGTCGACCTCGA-3'		
Vector1-rvs: 5'-GAATAATCTGTTTCGTGTCACTATTTGTTTG-3'		
Vector2-fwd: 5'-CAAACAAATAGTGACACGAAACAGATTATTC-3'		
Vector2-rvs: 5'-TCCTCGCCCTTGCTCACCATGCGGCCGCGGAGCC-3'		
canoe dsRNA primers	This study	N/A
5'-T7-AGCAGCAACAACACATCGAC-3'		
5'-T7-TTTTAATTTCTTGTCGCCCG-3'		
ephexin dsRNA primers	This study	N/A
5'-T7-CTTCCATGTTTACGTGGCCT-3'		
5'-T7-TGCACAGCAACAGAAGATCC-3'		
luciferase dsRNA primers	This study	N/A
5'-T7-GCGTAGCTTCCATCTTCCAG-3'		
5'-T7-TTTTCCGTCATCGTCTTTCC-3'		
Recombinant DNA		
PhiC31-UASp-GFP:CanoeRAΔNLS	This study	N/A
pAC-Gal4	Addgene	Cat #: 2344
UASp-Rap1Q63E (Rap1CA)	This study	N/A

(*Continued on next page*)

Continued

REAGENT or RESOURCE	SOURCE	IDENTIFIER
Software and algorithms		
MATLAB	MathWorks	https://www.mathworks.com; RRID: SCR_001622
FIJI	Schindelin et al.[81]	https://imagej.net/software/fiji/; RRID: SCR_002285
SIESTA	Fernandez-Gonzalez and Zallen[82]	https://doi.org/10.1088/1478-3975/8/4/045005
PyJAMAS	Fernandez-Gonzalez et al.[83]	https://doi.org/10.1093/bioinformatics/btab589
Original image analysis code	This study	https://doi.org/10.5281/zenodo.7893927

RESOURCE AVAILABILITY

Lead contact

Further information and requests for resources and reagents should be directed to and will be fulfilled by the lead contact, Rodrigo Fernandez-Gonzalez (rodrigo.fernandez.gonzalez@utoronto.ca).

Materials availability

The plasmids generated in this study are available from the lead contact upon request.

Data and code availability

- All data reported in this paper will be shared by the lead contact upon request.
- Original code used for image annotation and analysis is available at our lab website: https://www.quantmorph.ca/software. Custom scripts required to reanalyze the data reported in this paper have been deposited at Zenodo and are publicly available as of the date of publication. DOIs are listed in the key resources table.
- Any additional information required to reanalyze the data reported in this paper is available from the lead contact upon request.

EXPERIMENTAL MODEL AND SUBJECT DETAILS

Drosophila melanogaster lines (see key resources table) were raised in plastic vials/bottles at 22ºC or 25ºC, on fly food provided by a central kitchen operated by H. Lipshitz. Stage 14-15 embryos (12-14 hours after egg laying) were collected from apple juice-agar plates kept overnight at 22ºC on collection cages. There are no known differences in the physical and molecular mechanisms of collective cell movement during wound repair in male and female embryos, thus embryos were not distinguished based on sex. For live imaging and immunostaining, conditions are described in the method details.

Drosophila melanogaster S2R+ cells are male cells expressing the Wingless receptor derived from the S2 cell line cultured from late embryos (Drosophila Genomics Resource Center). Cells were maintained in 6 cm tissue culture dishes (Falcon) at 25ºC in Schneider's Drosophila Medium (Gibco) supplemented with 10% heat-inactivated fetal bovine serum (Gibco) and 1% antibiotic/antimycotic (Gibco). Cells were passaged every 3-4 days at a 1:4 split.

METHOD DETAILS

Fly stocks

We used the following markers for live imaging: *endo-DE-cadherin:tdTomato*,[39] *α-catenin:EGFP* MiMIC,[40] *rap1-GFP:Rap1*,[26] *endo-canoe:YFP*,[41,42] *UAS-GFP:canoeRAΔNLS* (Rap1 sensor, this study), *sqh-sqh:GFP*,[46] *zipper-zipper*:GFP,[47] *ubi-GFP:anillinRBD*,[50] *UAS-canoeWT:Venus* and *UAS-canoeΔRA:Venus* (gifts from Jennifer Zallen), *sqh-sqh:mCherry*,[49] *ubi-DE-cadherin:GFP*,[84] *UAS-diaRBD:GFP*,[52] *sqh-GFP:rok*^{K116A},[53] and *UAS-ephexin:YFP*.[75] Other UAS transgenes were *UAS-HA:rap1S17A* (Rap1DN) and *UAS-rap1Q63E* (Rap1CA),[76] *UAS-rap1-RNAi*,[77] *UAS-canoe-RNAi*,[77] and *UAS-rho1N19*.[51] *yellow white* flies, *UAS-mCherry-RNAi*,[77] and *UAS-ECFP-Golgi*[78] were used as controls. *daughterless-Gal4*[79] was used to drive UAS constructs, except for the Rap1 sensor, which was driven with *tubulin-Gal4*.[80]

Generation of Rap1 activity sensor

Components of the Rap1 activity sensor and vector backbone were generated by PCR from genomic DNA or plasmid DNA (vector containing PhiC31 integration sites, w+, UASp, and ampicillin resistance – gift from Mark Peifer) using the primer pairs listed in the key

resources table. The plasmid was assembled using Gibson Assembly.[85] The insert was introduced into a fresh vector backbone using BamHI and PspXI. The resulting plasmid was transformed into NEB 5-alpha Competent *E. coli*. and selected using Ampicillin. Resulting positive colonies were grown, DNA was extracted using QIAGEN Plasmid *Plus* Midi Kit, and verified using Sanger Sequencing (The Centre for Applied Genomics, SickKids).

The Rap1 activity sensor was tested for localization and functionality in S2R+ cells.[43] The Rap1 sensor was transiently transfected into the S2R+ cells using FuGENE (Promega) alongside AC-Gal4 (Addgene) and UASp-Rap1Q63E. Cells were plated on glass bottom dishes (Matsunami) coated with 0.5 mg/mL concanavalin A Type IV-S (Sigma-Aldrich) for live cell imaging. The final cDNA was sent to BestGene Inc for PhiC31 integration into $y^1w^{67}c^{23}$; P{CaryP}attP2 flies (BDSC #8622) and screening for *w*+ transformants. We used *tubulin-Gal4* to drive expression of the biosensor in the embryo.

dsRNA injections

Templates to produce dsRNA were generated by PCR from genomic DNA with primer pairs (key resources table) containing the T7 promoter sequence (5'-TAATACGACTCACTATAGGGAGACCAC-3') at the 5' end. PCR products were used as templates for the T7 transcription reactions with the MEGAscript T7 kit (Invitrogen). dsRNA was isolated using phenol/chloroform extraction and isopropanol precipitation.

For injections, embryos were collected for 60-90 min at 23°C, glued onto a coverslip, dehydrated for 12 minutes, and covered in a 1:1 mix of halocarbon oil 27 and 700. Embryos were immediately injected with dsRNA at the concentrations of 1.6 μg/ml (*luciferase* dsRNA), 0.3 μg/ml (*canoe* dsRNA), 1.3 μg/ml (*ephexin* dsRNA), or with ultrapure water. After injection, embryos were incubated at 18°C in a humidified chamber for 22 hours, at which time embryos were live-imaged.

Antibody staining

To validate Canoe knock down by *canoe* RNAi, stage 14 embryos expressing *daughterless*-Gal4 and either UAS-*mcherry*-RNAi or UAS-*canoe*-RNAi were dechorionated as above and fixed for 30 min in a 1:1 mix of heptane and 4% formaldehyde in PBS. Embryos were devitellinized manually. Staining was with primary antibodies rabbit anti-Canoe (1:1000, gift from Mark Peifer) and mouse anti-Dlg (1:500, Developmental Studies Hybridoma Bank) and secondary antibodies goat anti-rabbit Alexa 488 (1:500, Invitrogen) and goat anti-mouse Alexa 568 (1:500, Invitrogen). Embryos were mounted in Prolong Gold (Molecular Probes) between two coverslips. Stained embryos were imaged at 60X magnification on an Olympus FluoView 3000 laser scanning confocal microscope. Canoe intensities were normalized to the Dlg signal for quantification of Canoe knockdown.

Time-lapse imaging

Stage 14-15 embryos were dechorionated in 50% bleach for 2 min, rinsed, glued ventral-lateral side down to a glass coverslip using heptane glue, and mounted in a 1:1 mix of halocarbon oil 27 and 700 (Sigma-Aldrich).[86] Embryos were imaged at room temperature using a Revolution XD spinning disk confocal microscope equipped with an iXon Ultra 897 camera (Andor, Belfast, UK), a 60x oil immersion lens (Olympus, NA 1.35) and Metamorph software (Molecular Devices). Sixteen-bit Z-stacks were acquired at 0.5 μm steps. Maximum intensity projections were used for markers that localized strongly to the apical surface of cells. For markers that localized throughout the cells (e.g. Rap1:GFP, Rap1 activity biosensor, or Ephexin:YFP), LocalZProjector[87] was used to identify the apical surface of the embryos and create a maximum intensity projection of the 3 planes surrounding the apical plane. To minimize environmental changes (temperature, humidity, etc.) that could affect our results,[88] we completed control and experimental groups for each experiment within two weeks.

Laser ablation

Laser cuts were conducted using a pulsed Micropoint nitrogen laser (Andor Technology) tuned to 365 nm. For wounding, 10 pulses were delivered at discrete spots 2-μm apart along a 13-μm line. Each embryo was wounded only once. For spot laser ablations, 10 pulses were delivered at a single point over the course of 670 ms. The tissue was imaged immediately before and after ablation, and every 4-30 s.

QUANTIFICATION AND STATISTICAL ANALYSIS

Quantitative image analysis

Image analysis was done in FIJI,[81] SIESTA[82] and PyJAMAS.[83] To delineate the wound margin, we used the semiautomated LiveWire algorithm that identifies the brightest pixels between two manually selected points. To quantify fluorescence in time-lapse images, we used a 0.5-μm-wide mask generated from the wound margin traces. Intensity values were background-subtracted using the image mode as the background and corrected for photobleaching by dividing by the mean image intensity at each time point. We quantified myosin heterogeneity at time t as:

$$heterogeneity(t) = \frac{\sigma(t)}{\mu(t)}, \quad \text{(Equation 1)}$$

where $\sigma(t)$ and $\mu(t)$ are the standard deviation and mean, respectively, of the pixel values under the wound edge annotation at time t.[14] To measure TCJ intensity over time, fiducials were manually placed on 5-12 TCJs per embryo. Intensity at each TCJ was extracted

using a circular mask 0.5 μm in diameter. TCJ intensities were corrected as above. To measure BCJ intensity over time, individual interfaces between wounded and adjacent cells were delineated as segments of the identified wound edge between two adjacent TCJs. Each interface was divided into 1000 evenly spaced points and fluorescence was quantified using linear interpolation.[18] BCJ intensity was calculated as the mean of the central 200 points. Intensity values were corrected and normalized as above.

To measure retraction velocity after laser ablation, the positions of the two TCJs connected by the ablated junction were manually tracked. The instantaneous recoil velocity was calculated as the change in distance between TCJs divided by the length of time between acquisition of the pre-cut and post-cut images. To estimate changes in viscoelastic properties between different experimental groups, we modelled cell junctions as viscoelastic elements using a Kelvin-Voigt circuit.[54] A Kelvin-Voigt element models the damped recoil of an elastic material as:

$$L(t) = \frac{\sigma_0}{E}\left(1 - e^{-t\left(\frac{E}{\mu}\right)}\right) = D\left(1 - e^{-\frac{t}{\tau}}\right), \quad \text{(Equation 2)}$$

where $L(t)$ is the distance between the TCJs at time t after ablation, σ_0 is the tension sustained by the junction, E is the elastic coefficient, and μ is the viscosity. Fitting laser ablation experiments with Equation 2 allows estimation of D, the asymptotic value of L, proportional to the tension sustained by the junction, and τ, a relaxation time that depends on the viscoelastic properties of the cell junction.

Statistical analysis

We did not assume data to be normally distributed; therefore we used non-parametric statistical tests. To measure significance of changes compared to zero, we used a one-sample Wilcoxon signed-rank test. To compare data at two time points, we used a paired two-sample Wilcoxon signed-rank test. We compared sample means between two independent groups using a non-parametric Mann-Whitney test. To compare more than two groups, we used a Kruskal-Wallis test to reject the null hypothesis and Dunn's test for pairwise comparisons.